AD-A178 746 MODIFICATIONS TO THE INLET FLOW FIELD OF A TRANSONIC COMPRESSOR ROTOR(U) EXOTECH INC CAMPBELL CA F NEUHOFF DEC 85 TR-0503 NPS-67-85-008CR 1/1

UNCLASSIFIED F/G 21/5 NL

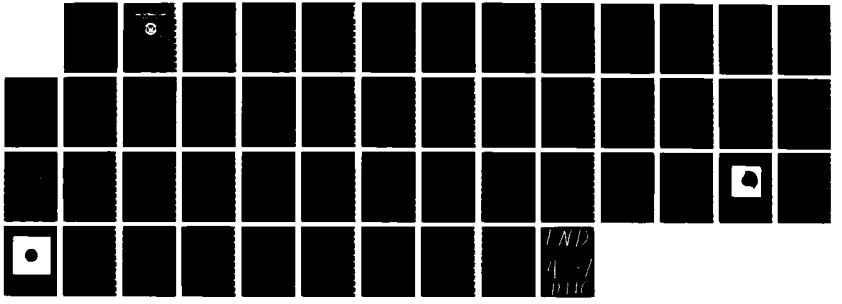

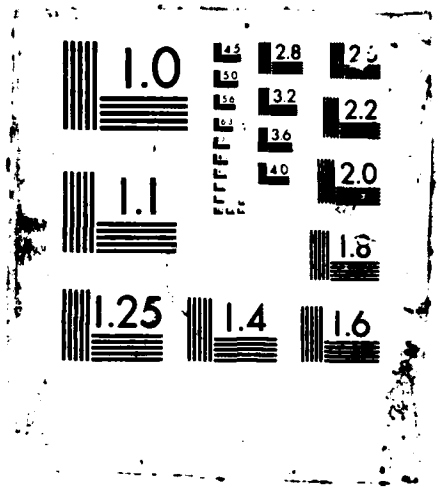
1.0
1.1
1.25
1.4
1.6
1.8
2.0
2.2
2.8
3.2
3.6
4.0
4.5
5.0
5.6
6.3

NPS67-85-008CR

NAVAL POSTGRADUATE SCHOOL
Monterey, California

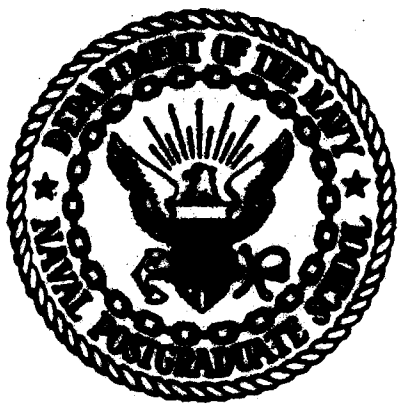

CONTRACTOR REPORT

MODIFICATIONS TO THE INLET FLOW FIELD OF A TRANSONIC COMPRESSOR ROTOR

F. NEUHOFF
EXOTECH INC.
1901 S. BASCOM AVENUE, SUITE 337
CAMPBELL, CALIFORNIA 95008

JULY 1985

FINAL 1 JUNE 1985 - 31 JULY 1985

Prepared for:
Naval Postgraduate School
Monterey, CA 93943

REPORT DOCUMENTATION PAGE

1a REPORT SECURITY CLASSIFICATION: UNCLASSIFIED	1b RESTRICTIVE MARKINGS
2a SECURITY CLASSIFICATION AUTHORITY	3 DISTRIBUTION/AVAILABILITY OF REPORT: Approved for Public Relaease; Distribution Unlimited
2b DECLASSIFICATION/DOWNGRADING SCHEDULE	
4 PERFORMING ORGANIZATION REPORT NUMBER(S): TR 8503	5 MONITORING ORGANIZATION REPORT NUMBER(S): NPS67-85-008CR
6a NAME OF PERFORMING ORGANIZATION: Exotech Inc. / 6b OFFICE SYMBOL (If applicable)	7a NAME OF MONITORING ORGANIZATION: Department of Aeronautics
6c ADDRESS (City, State, and ZIP Code): 1901 S. Bascom Ave. Ste 337 Campbell, CA 95008	7b ADDRESS (City, State, and ZIP Code): Naval Postgraduate School Monterey, CA 93943
8a NAME OF FUNDING/SPONSORING ORGANIZATION / 8b OFFICE SYMBOL (If applicable)	9 PROCUREMENT INSTRUMENT IDENTIFICATION NUMBER: N6237685WR00018
8c ADDRESS (City, State, and ZIP Code)	10 SOURCE OF FUNDING NUMBERS: PROGRAM ELEMENT NO: 62241N; PROJECT NO: ; TASK NO: ; WORK UNIT ACCESSION NO: WR00018

11 TITLE (Include Security Classification)
Modifications to the Inlet Flow Field of a Transonic Compressor Rotor

12 PERSONAL AUTHOR(S)
Friedrich Neuhoff

13a TYPE OF REPORT	13b TIME COVERED	14 DATE OF REPORT (Year, Month, Day)	15 PAGE COUNT
Final	FROM 1JUN85 TO 31JUL85	DEC 1985	54

16 SUPPLEMENTARY NOTATION

17 COSATI CODES		
FIELD	GROUP	SUB-GROUP

18 SUBJECT TERMS (Continue on reverse if necessary and identify by block number)
Transonic Compressor, Inlet Flow Field, Distortion Screens,

19 ABSTRACT (Continue on reverse if necessary and identify by block number)

The flow to the rotor of a single stage axial transonic compressor was found to be in disagreement with design requirements. The incidence angle to the rotor blading was measured to be towards stall in the hub and tip regions when close to design near center-span. Hardware modifications were made, guided by flow field calculations, and predictions were compared with measurements. The most significant improvement was obtained by increasing the flow rate at open throttle. No practical method to correct the flow near the hub was found.

20 DISTRIBUTION/AVAILABILITY OF ABSTRACT	21 ABSTRACT SECURITY CLASSIFICATION
☐ UNCLASSIFIED/UNLIMITED ☐ SAME AS RPT ☐ DTIC USERS	UNCLASSIFIED
22a NAME OF RESPONSIBLE INDIVIDUAL: R. P. SHREEVE	22b TELEPHONE (Include Area Code): (408)646-2593 / 22c OFFICE SYMBOL: 67Sf

DD FORM 1473, 84 MAR — 83 APR edition may be used until exhausted. All other editions are obsolete.

TABLE OF CONTENTS

List of Figures

I. Introduction

To gain a better understanding of the rather complex loss mechanisms involved in transonic compressor rotors, an experimental program was initiated using a small single stage axial compressor of in-house design. The compressor is shown in Fig. 1 and is described in Ref. 1. The compressor and test rig, was designed in the late 1960's by Dr. M. H. Vavra, not as a state-of-the-art compressor stage, but to provide a tool to produce and to understand transonic flow phenomena. Operating the machine at lower than design speeds (up to 70% of referred design speed), fairly high overall efficiencies were measured. From detailed rotor blade-to-blade measurements at the rotor exit, using a newly developed measurement technique (Ref. 2), it was found that the rotor blade wakes of the hub and tip regions were rather large and very unsteady. The rotor in and outflow was measured using radially traversing combination probes (Ref. 3). These probes resolved the average velocity vector in magnitude and direction as well as the local average total temperature.

In the design, rotor blading shapes were defined on five conical surfaces, each separating 25% increments of the total mass flow from hub to tip. Through integration of the measured mass flux distribution from hub to tip, the assumed streamline distribution was verified closely. Also the pitch angle variation over the blade span agreed quite well with the design (Fig. 2). The disagreement in pitch angle measurement compared to design in the tip region was the result of measurement error due to case wall influence. A further assumption made in the design was that the axial component of the inlet velocity would be constant over the blade height. Figure 3 compares the assumed and measured distributions. They clearly differ substantially, especially in the hub and tip regions. Since the measured pitch angle

distribution across the inlet radius agreed quite well with the design distribution, a discrepany in the axial velocity component will imply a discrepancy in the relative inlet angle β_1. Also during the design process, a calculational error had been made in the calculation of the blade stagger angle. The incidence angle (i) was added instead of subtracted in calculating the stagger angle to which the blades were set. When the rotor was built, with camber angle and stagger angle then fixed, in order to keep the incidence angle close to the minimum loss setting, the relative inlet angle β_1 would be changed. Since there are no inlet guide vanes, the flow to the rotor is in axial planes, and β_1 is determined by the rotor peripheral speed and the meridional absolute velocity. For a given speed β_1 can only be changed by varying the absolute velocity. Changing β_1 leads to a change of the minimum loss incidence angle. Calculation showed that the minimum loss incidence angle would vary some $\pm 1^{\circ}$ about the original value.

Figure 4 shows the originally intended distribution of air inlet angle compared to the one which is required by the rotor as built. Also shown is the design incidence angle with a deviation of $\mp 1^{\circ}$ indicated. Using the corrected β_1 and the wheel speed, the axial velocity component was recalculated. Figure 5 shows a comparison between the calculated axial component and the measured one (as in Figure 3). The flow field required to satisfy the rotor as-built differs even more from what is measured than does the original design distribution. The measured relative inlet angle (β_1) is compared to the one the blading optimally requires in Figure 6. The significance of the design discrepancy becomes most obvious in the comparison of measured and required incidence angles, also shown in Figure 6. Figure 7 shows the profile loss versus incidence angle for a profile similar to the rotor hub profile. The minimum loss incidence angle is almost

independent of inlet Mach number. The operating range however narrows drastically with increasing inlet Mach number. Since the inlet Mach number at 60% of design speed was 0.7 at the tip and the distribution of the relative inlet angle β_1 was observed to be independent of machine speed (at constant throttle), it was reasoned that if the inlet flow field could be improved experimentally at low speeds, the flow would be acceptable at the more critical high speed conditions. In the following paragraphs, an account is given of attempts which were made to improve the inlet flow field including modifications to the flow path geometries and the use of radial distortion screens. The finite difference program, MERIDL, was used to predict the effect of changes in the flow path.

II. Inlet Modifications Calculated & Measured

Hardware modifications and testing can be time consuming and costly. On the other hand, proven computer codes can provide fast and inexpensive predictions of the effects of modifications. To be able to rely on calculations however, one has to examine the accuracy achievable with the code. Hence a comparison was made, at 60% of design speed, between the axial velocity component which was measured at the rotor inlet with that calculated using the inviscid finite difference code, MERIDL (Ref. 5). The code was used for the inlet flow only and not for the flow through the compressor itself. Figure 8 shows the results. There is some disagreement near the outer case-wall (blade tip), since the code does not include the boundary layer, and no measurement data are available near the hub, since the probe could not be traversed closer than 0.25 inches to the hub wall, but overall the agreement for the blade span is good. For each of the following hardware changes which were made and tested, the corresponding calculations made using MERIDL are also described.

II.1 Small Radius Inlet Contraction

In the original arrangement, the inlet to the compressor was an 18 inch diameter pipe which was subsequently reduced to an 11 inch compressor case wall diameter through a bellmouth contraction. The beginning of the contraction was located 21 inches upstream of the rotor leading edge. The 18 inch diameter supply pipe extended upstream to the flow nozzle (15ft.). Within the 18 inch pipe a substantial boundary layer would be present and the smooth bellmouth contraction would allow this boundary layer fluid to be evenly accelerated into the compressor casewall region. To prefentially accelerate the low energy fluid, the bellmouth was replaced by a small radius contracting nozzle (Figure 9). The small fillets shown at the spinner tip, at the end of the 18 inch diameter pipe, and at the beginning of the contraction were present and necessary in the calculation only.

The modified inlet at 60% of design speed, resulted in an increase of 6% in the mass flow rate at open throttle. Figure 10 shows the radial distributions of axial velocity which were measured and calculated. The qualitative distribution over the blade span showed little change. The increase in mass flow rate increased the level of the profile compared to Figure 8. Agreement between calculation and measurement was good, except for the tip area again. In the center portion of the span, the measured incidence angle (Figure 11) was fairly close to what is required optimally by the rotor. The hub and tip still showed large departures. Qualitatively, the incidence angle distribution over the blade span was not changed.

II.2 Small Radius Inlet Contraction with a Conical Screen

In Figure 8, there is a decrease in the flow rate toward the hub. The first inlet modification did not change this profile (Figure 10). In order to

deflect the flow into the center of the inlet, a conical screen was added to the small radius contracting nozzle. Located as shown in Figure 12 a screen of fairly low blockage was designed to turn the flow towards the centerline without incurring unacceptable losses. The configuration was investigated experimentally. The loss in total pressure measured across the screen was small, resulting in only a small drop in the flow rate. The change in the axial velocity component distribution over the blade span (Figure 13) showed only insignificant improvements compared to the no screen configuration. The peak value of the velocity was shifted slightly towards the compressor centerline. Towards the casewall a more distinct drop in velocity was observed. However, the changes achieved were small and did not achieve the desired velocity distribution. Further modifications of the conical screen arrangement were therefore not attempted.

II.3 Nozzle Type Contraction at Casewall Ahead of the Rotor

In order to accelerate and deflect the flow toward the center of the inlet, casewall contractions ahead of the rotor were investigated. Different nozzle shapes were either analyzed using MERIDL, or built and tested. Figure 14 shows a cross-section through the inlet including one nozzle. The calculated version differed slightly from the geometry which was built since the leading edge could not be manufactured with reasonable effort. Also a small difference in the nozzle throat diameter occurred. In both calculated and tested geometries the trailing edge of the nozzle was located 1.5 inches upstream of the rotor leading edge. Figure 15 shows the calculation region for the configuration and shows the nozzle position with respect to the rotor inlet. The results of measurement and calculation are shown in Figure 16. They depart somewhat from each other, perhaps due to the differences in

geometry. The measured nozzle created a reduction in outer casewall velocity, which was only regained gradually towards the center of the inlet. The peak value changed insignificantly. The calculated nozzle produced a more uniform distribution of axial velocity component for the outer half. There was a slight increase in velocity near the center of the inlet, but the general shape of the velocity distribution was not changed. From several comparisons between calculations and measurements sufficient confidence was gained in the computer code that more inlet variations were calculated without testing.

III. Calculated Inlet Modifications

In the following, inlet modifications which were only calculated are presented. Some modifications (III.2 especially) would have required difficult hardware changes. For this reason, the proven computer code was very valuable, since it eliminated the need for both hardware modification and testing.

III.1 Constant Cross-Section Nozzle in the Inlet

From the calculations for the first contracting nozzle it was observed that a reduction of inlet area ahead of the rotor can produce a more uniform axial velocity distribution over the blade height. Calculations at a station some 8 inches upstream of the rotor leading edge, where the inlet duct was strictly cylindrical, predicted that the axial velocity was constant over the channel height. Since the spinner contraction was found to be an important influence on the velocity distribution at the rotor leading edge, a case wall nozzle was designed that had its throat slightly ahead of the spinner tip and ended at the rotor leading edge. The nozzle throat area was equal to the rotor face area. From the nozzle throat to the rotor leading edge, the area was not changed in the direction of the machine axis. This was done such

that, for the outer half of the blade span, the area perpendicular to the case wall was constant; and for the inner half, the area perpendicular to the hub contour was constant. The contraction of the nozzle to the throat was a simple continuous curvature. A calculation was made using the same mass flow rate as for the first nozzle configuration. Figure 18 shows the calculated axial velocity distribution. There was a distinct non-uniformity in the distribution. A pronounced peak value occurred at approximately the center of the passage, with an almost symmetrical drop-off at both ends (hub and tip). The velocity gradient in the tip region was more pronounced than before. The hub velocity was increased, but the intended uniformity over the passage height was not achieved. Figure 19 shows the corresponding incidence angle distribution. The incidence angle was reasonable for the center portion of the blade. The disagreement for the rest of the span was unchanged.

III.2 Centerbodies

The original rotor spinner was a round, rather blunt shape (Figure 1). The hub contour forced the flow to turn from axial to a pitch angle of 40° to the axis at the rotor leading edge, within a fairly short distance. A change in passage cross-sectional area of 25% occurred within 1.5 inches (or 27% of the blade height). There was reason to believe that a near stagnation region ahead of the spinner would be developed, which would cause a substantial volume of flow to slow down unnecessarily. To eliminate this effect, centerbodies of different diameters extending some 20 inches upstream of the rotor leading edge were examined. The most successful version is shown in Figure 20. The diameter was slightly smaller than the hub diameter at the rotor leading edge. A straight cone initiated the center body at the axial location where the bellmouth contraction began. In Figure 21 the axial

velocity component for this configuration is shown. Although a more constant distribution for the upper 50% of the blade span was achieved, the strong gradient at the hub was not overcome. It is noted that the axial station corresponding to the results of Figure 21 is 0.47 inches downstream of the end of the centerbody. At that particular location, the hub was sloped at 40°. Also shown in Figure 21 are the axial velocity components at three further upstream locations. At the locations where the centerbody was strictly cylindrical (Stations 1 & 2, Figure 20), the distribution is almost flat. Yet at station number 3, where the spinner slope began, a distinctly non-uniform axial velocity profile was apparent. Centerbodies of smaller diameter showed the same tendencies more clearly. Larger diameters were not calculated, since it was not possible to incorporate such hardware changes into the test rig.

III.3 Conical Spinner

As mentioned in III.2 the spinner was rather blunt and produced a substantial stagnation area in the center of the flow. To reduce the stagnation effect, a strictly conical spinner design was calculated. The hub meridional angle at the rotor leading edge of 40° was maintained from the leading edge of the rotor forward to the tip of the spinner. A very small fillet had to be incorporated to accomplish the transition from axial at the point of the spinner. Figure 22 shows the calculation region, together with the original spinner. The corresponding calculated axial velocity component distribution is shown in Figure 23. Also plotted is the distribution for the original round spinner. There were only small differences between the two geometries. In Figure 24 the radial distributions of pitch angle at some 0.375 inches ahead of the rotor are compared. Here again only small changes were found. Since the axial velocity and the pitch angle distributions did not change, then the streamlines also did not change. It should be mentioned

that in the calculation of the original spinner, a fairly large fillet had to be used (Figure 9), since the program could not handle 90° changes in (surface) slope.

IV. Inlet Screens

The attempts to generate the inlet flow field required by the rotor described so far attempted to modify the flow without generating additional losses (except for the conical inlet screen, II.2). While an increase in mass flow rate of up to 6% (II.1) was achieved, the general shape of the velocity distribution was not altered. In the following some hardware modifications are described, which were only tested, but not calculated. The velocity profile needed (Figure 5) is the opposite of what one would expect in an empty channel with walls fed from a constant pressure. To achieve higher velocities at hub and tip, more mass flow should be fed to these regions. As the existing hardware did not allow modifications close to the rotor front face, changes to the inlet 10 inches upstream of the rotor leading edge were effected. In order to generate flow areas with different velocities, partial blockage of the passage by wire screens of various sizes and blockage coefficient were examined. The intent was to generate concentric jets with different velocities, which would mix to cause smooth velocity gradients. From free jet investigations (Reference 7) it was known, that jet mixing occurred in plumes with a half angle spread rate of 6° (Figure 25). Although the case discussed here and shown in Figure 26 was different from that described in Reference 7, in that there are concentric jets of different velocities mixing rather than one jet mixing with ambient static conditions, for design purposes it was assumed that mixing would still spread at a half angle of 6°. As the cross-section downstream of the screen perpendicular to the flow was not constant, the plumes were represented by the area ratio

corresponding to an increase or decrease as would occur in a straight duct. Figure 26 is a sketch of the hardware arrangement with the desired velocity profile. Six thin wires were strung across the annulus and an annular mesh was attached to it. The mesh created a blockage which slowed the flow locally while the flow which by-passed the mesh area retained full stagnation pressure. The inner and outer diameter of the mesh were calculated such, that the velocity at the hub and outer case walls just began to fall at the rotor leading edge. Velocity gradients at hub and tip, are joined to a low speed core portion. The blockage of the mesh, defined as the loss of total pressure with respect to freestream dynamic pressure, was varied in the design procedure, together with the axial and radial dimensions.

IV.1 First Inlet Screen

Figure 27 shows the first version of an inlet screen positioned in the inlet duct. The blockage was 0.430, the inner diameter was 4 inches and the outer diameter 10 inches, leaving a 0.5 inch gap at the casewall. The screen was held in the duct shown in Figure 9, mounted ahead of the compressor inlet. The duct was the same diameter as the compressor inlet and transitioned smoothly. The mesh itself was located 10 inches upstream of the rotor leading edge. With the small radius inlet nozzle as shown in Figure 9, the configuration was tested at 60% of design speed. Figure 28 shows a comparison of the axial velocity component for the same inlet configuration, with and without the inlet screen. There was a measurable change in the tip region. The outer part of the flow was accelerated and had a velocity gradient opposite to that measured previously. For a small area near the hub there was also a noticeable increase in velocity, but are over too small an area. It was concluded that the outer diameter of the mesh should be reduced so that

more high velocity flow could reach the rotor leading edge at the blade tip. At the same time, the inner diameter should be enlarged so that the hub flow would also be increased. To increase the velocity gradient the blockage of the mesh was also increased.

IV.2 Second Inlet Screen

A second version of the inlet screen was manufactured. At a blockage of 0.866 the inner diameter was enlarged to 5.4 inches and the outer diameter reduced to 9.6 inches. Figure 29 shows the new screen installed. The results for otherwise indentical running conditions are shown in Figure 30. The velocity gradient for the upper 50% of the blade span closely approximated the required gradients. There was however a velocity gradient in the wrong direction in the hub area. Figure 31 shows that the incidence angle in the tip region was fairly close to the design minimum loss incidence angle. In the hub area the difference in incidence angle exceeded five degrees. Since the tip experiences much higher relative inlet Mach numbers than does the blade root, and the blade-element performance at the tip is correspondingly more sensitive to incidence errors, further attempts were directed mainly towards correcting the tip flow. Accepting that the hub velocity profile could not be changed easily, the best method to improve the tip flow was to increase the overall flow rate. Thus the complete velocity profile would be shifted towards higher values, moving the incidence angle into the desired range. The data shown so far were for full open throttle. An increase in flow rate at unchanged rotor speed could only be achieved by relieving the pressure drops upstream or downstream of the rotor. From the measurements, the inlet ducting generated only small losses in total pressure. The area ratio of inlet-throttle plate to the compressor front face was large. Thus

the velocity through the open throttle was small, causing only minor losses. As shown in Figure 1, a honeycomb flow straightener was installed downstream of the stator, followed by a radial diffuser. Earlier tests had shown that the flow out of the stator was not axial but contained swirl angles of up to 10°. The losses that would be generated by the flow straightener were calculated and measured to be fairly large. On the other hand, the performance of the radial diffuser was calculated not to change much if the flow was swirling or if the flow straightener was removed altogether. For these reasons, the honeycomb section was removed. For the same inlet screen and rotor speed an increase in mass flow rate of 5.4% was subsequently measured. The inlet velocity profile did not differ in shape however from the one previously measured (Figure 32). The velocity magnitudes increased, rather uniformly, across the blade span. For the tip, the improvement was the most significant. Overall, the improvement was small. The increase in flow rate required to move the velocity profile to achieve optimum incidence was still quite large.

Other hardware changes to increase the open throttle, involving flow rate and the compressor outlet section, were considered. Eight 3/4 inch diameter bolts separate and space the inner and outer walls of the radial diffuser. The bolts are faired in a reasonble manner for swirl-free flow. They block 10% of the diffuser area where they are located. This represents a reasonable decrease in flow area, if the flow is with the radial, but could imply a much larger blockage and losses when the flow is swirling at high incidence to the fairings. To change this arrangement however, would have required a substantial amount of hardware modification. The effort was estimated to be out of proportion when compared to the possible gain, and was not pursued further.

IV.3 Third Inlet Screen Modification

The results in IV.2 suggested that, if the center opening were further enlarged, a higher value of axial velocity would be achieved near the hub. Similarly a reduction of the outer radius would allow more flow near to the case wall, leading to a further increase in velocity at the tip. The existing screen was modified to have an inner diameter of 7.3 inches and an outer diameter of 9.6 inches. The blockage was unchanged. Figure 33 shows the axial velocity component distribution which was measured for open throttle running conditions. The velocity magnitude near to the hub was basically unchanged, as was the velocity gradient. Towards center span where the velocity reached a maximum, the value was very close to the requirement. An immediate drop, however ingoing toward the tip produced low velocities for the outer 40% of the span. The second peak, towards the tip, was smaller than for the larger diameter screen. Thus the goal to speed up the flow in the tip region was not achieved, while a slight improvement toward the hub region was realized. A change of the velocity gradient toward the hub however did not occur.

In order to assess the throttling effect of the screen just described, the screen was removed and the compressor run at the same speed and open throttle. An increase in flow rate of 5% was measured. The rotor inlet velocity profile shown in Figure 34 indicated that the third screen merely blocked the flow over 28% of the span near the center. The gain in the level of velocity near the hub and tip was quite small compared to the unrestricted inlet. Therefore, while a radial velocity profile qualitatively similar to the requirement was achieved, an inlet without any mesh was better overall. It allowed the axial velocity to be closer to its optimum value over a larger fraction of the outer 60% of the span.

In reviewing the inlet screen variations it was concluded that, it is indeed possible to increase the velocity near to the tip. The smaller the gap between screen and the casewall, the larger the increase obtained. No screen however could effectively change the radial velocity gradient in the hub area. The flow there is clearly determined by the contour of the spinner. If a sizeable increase in flow rate (20% to 25%) were possible, screen configurations like those described in IV.1 and IV.2 would be clearly advantageous. Since it was quite impractical to achieve this in the current test rig, it was more practical to have the compressor operate at close to correct inflow for the greater part of the span, rather than with large departures for almost all of the span. No further inlet screens were investigated.

V. Conclusions

The successful application of the flow code MERIDL and the results of the associated test program showed that wall geometry changes could not be used effectively to produce the radial distribution of meridional inlet velocity which was required optimumly for the compressor rotor, as built.

It was also shown experimentally that a radial distortion screen could, if optimized, produce the required radial profile. However, the losses associated with the use of a screen results in an overall reduction in the open-throttle flow rate. Consequently, while the profile shape might be correct, the level of velocity would be everywhere too low to give acceptable incidence angles.

The required increase in the overall level of open-throttle flow rate which would permit the use of a screen might be achieved in three ways, namely;

(i) use of an auxiliary compressor in series

(ii) redesign of the stator to better match the rotor

(iii) improve the diffuser performance.

In view of the expense involved in (i) - (iii), operation of the present rotor to higher speeds without screens (which gives the closest approach to correct incidence over the outer span), is recommended. This will allow extension of velocity field measurements to higher transonic Mach numbers and permit the shock structure at the tip to be examined and compared with cascade results.

A rotor or complete stage redesign should preceed flow field mapping for code verification purposes.

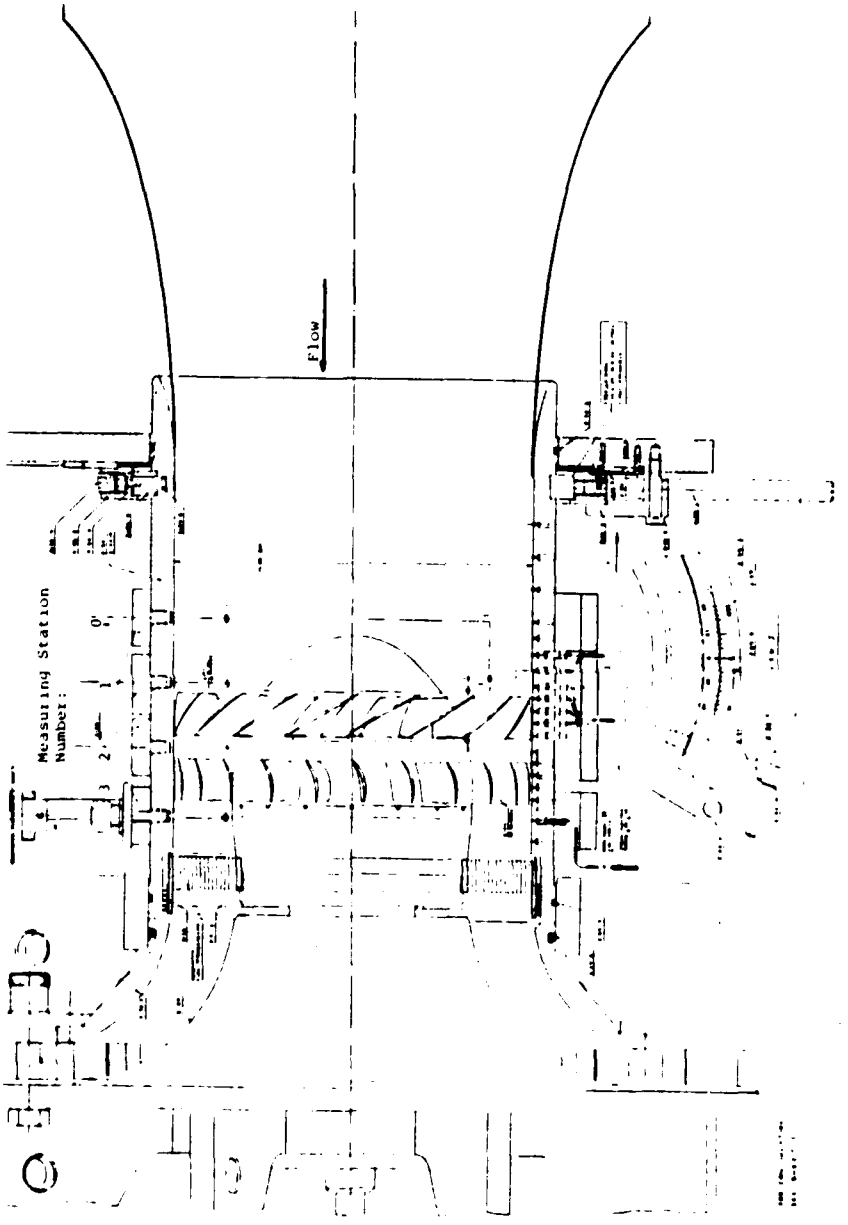

Figure 1. Transonic Compressor Test Rig

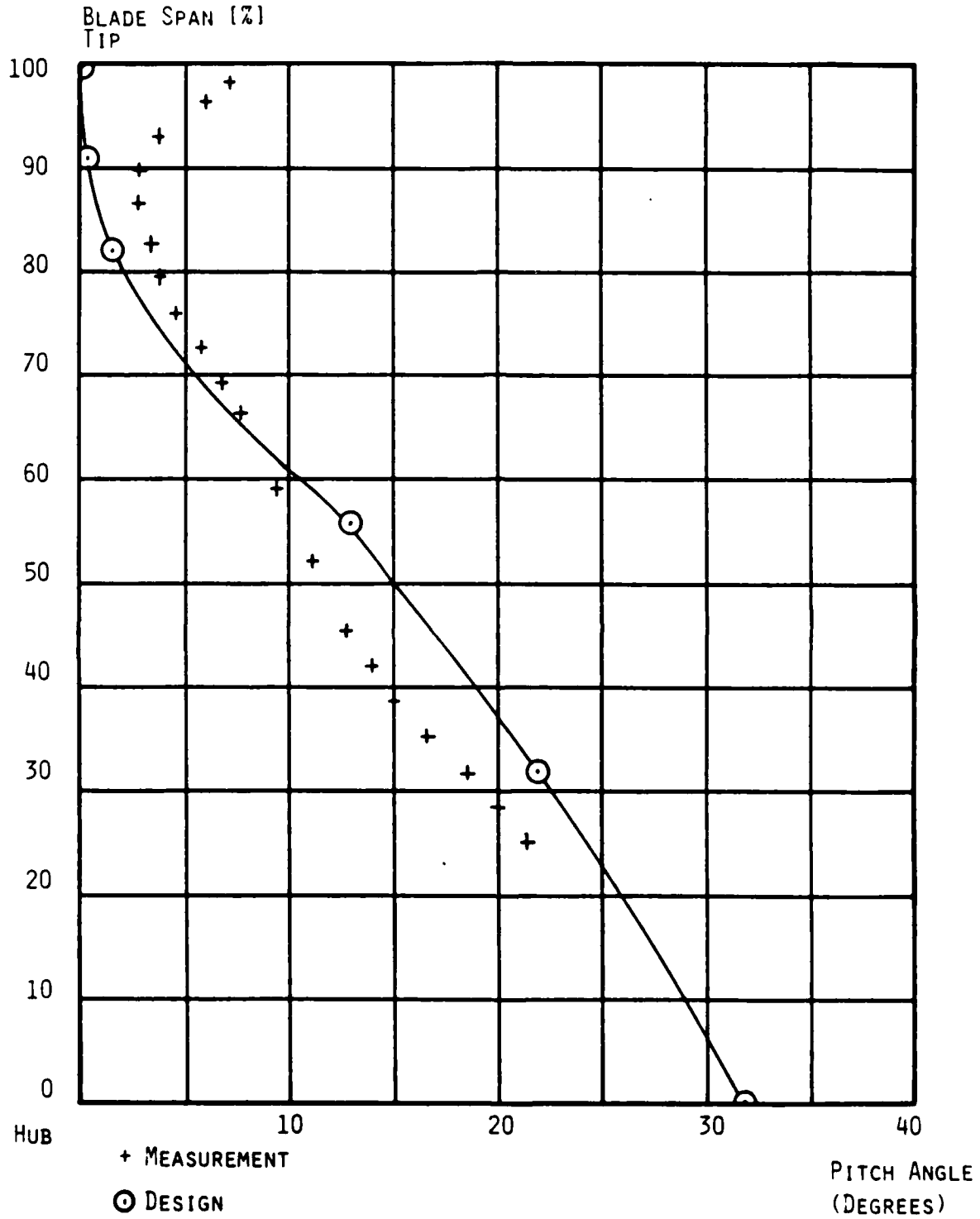

Figure 2. Radial distribution of flow pitch angle at rotor inlet.

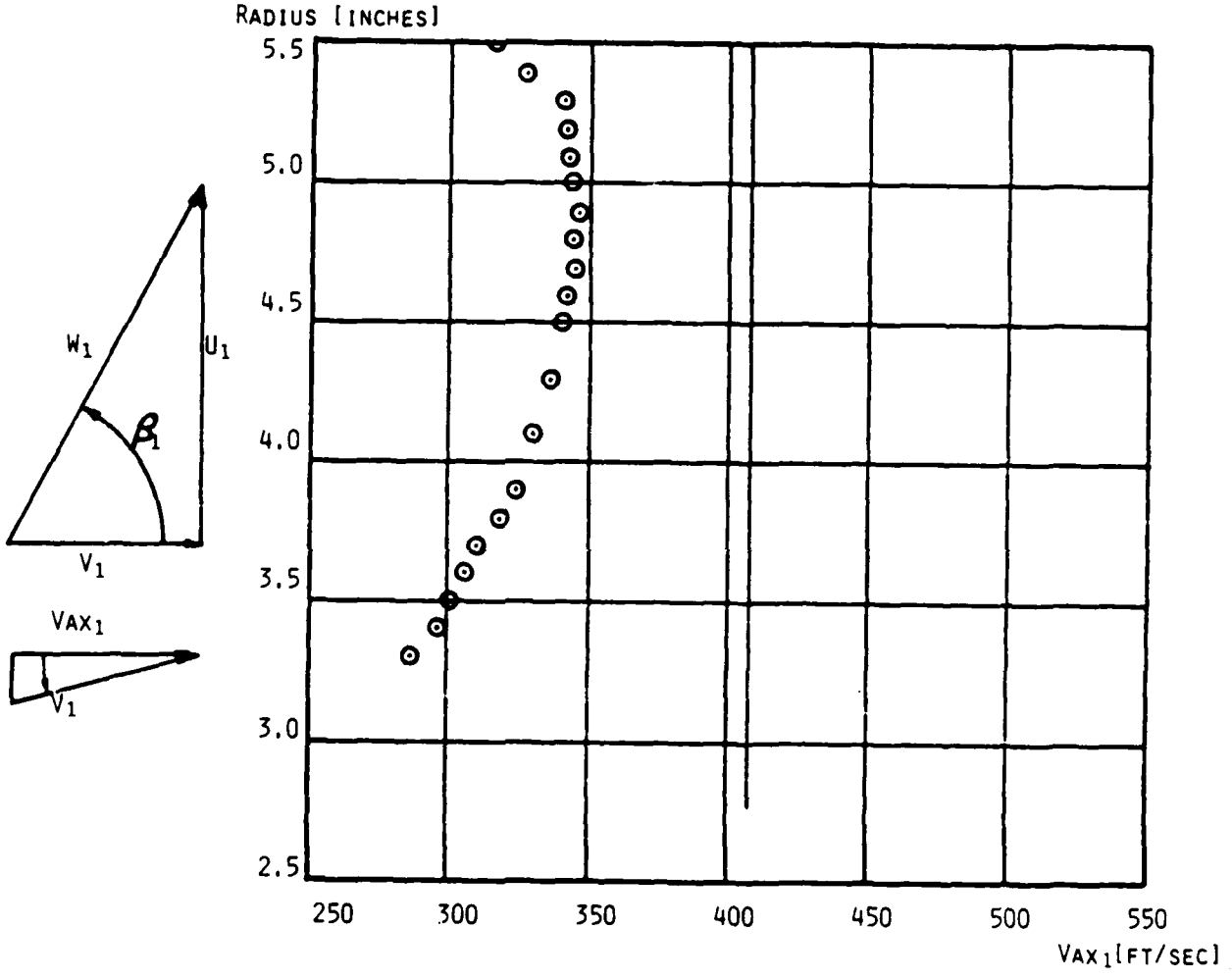

Figure 3. Radial distribution of axial velocity component at rotor inlet. Measurement (symbols), original design requirement (straight line).

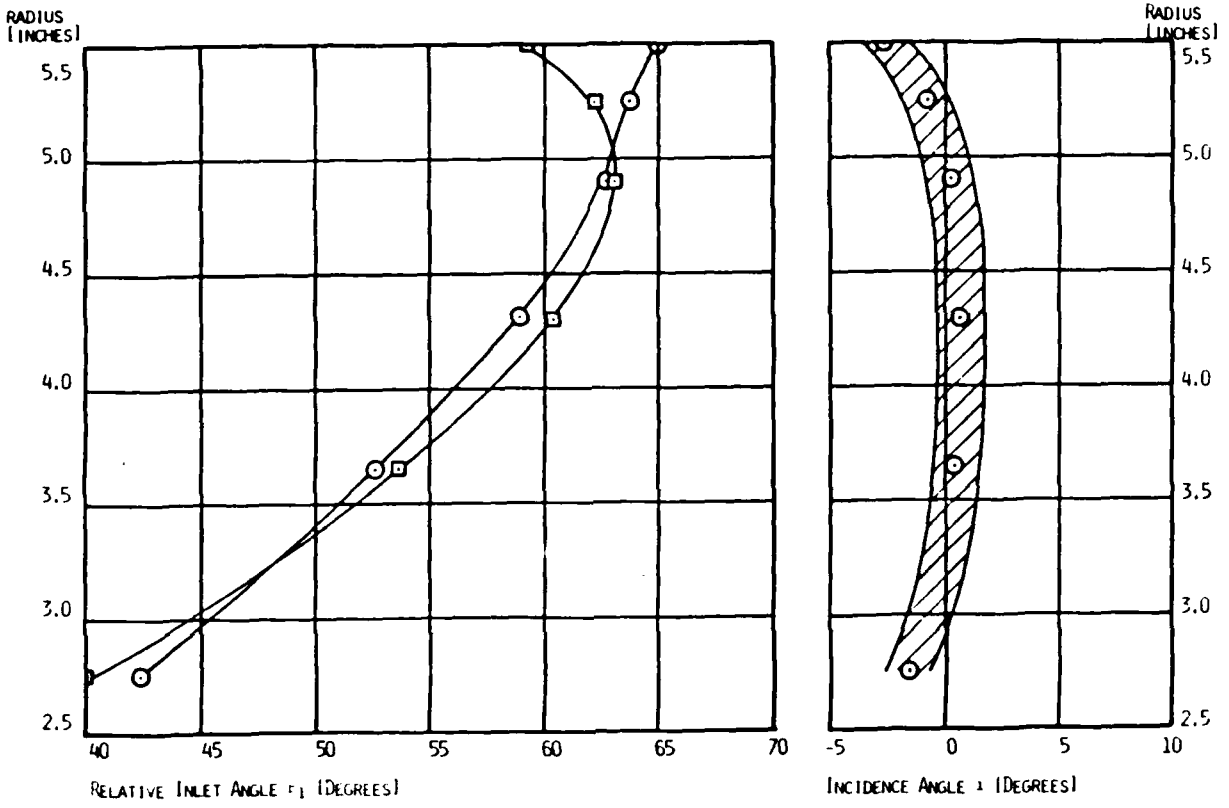

⊙ Original design requirement

⊡ As-built requirement

Figure 4. Relative rotor inlet angle β_1 and incidence angle versus radius.

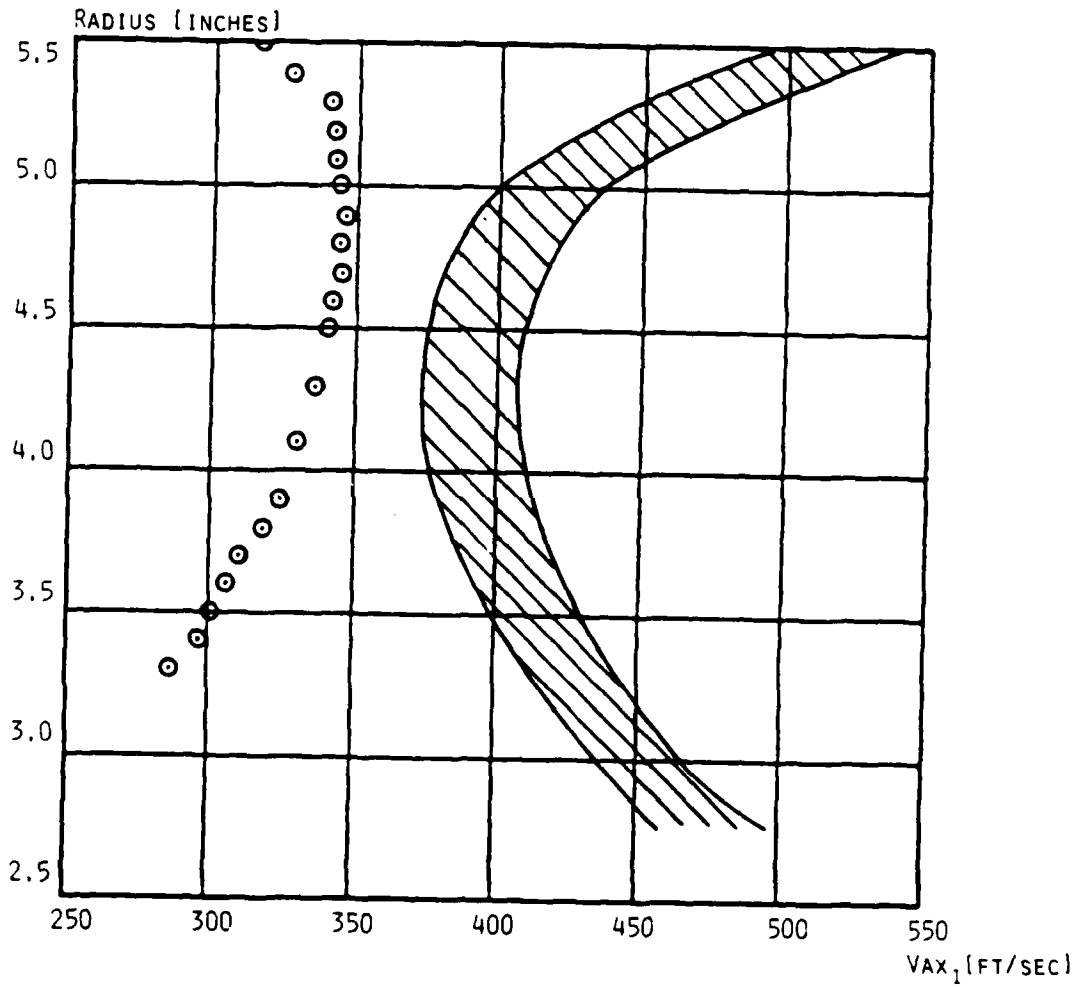

Figure 5. Radial distribution of axial component of inlet velocity (Vax_1); measured ⊙ ; required for optimum incidence (shaded area).

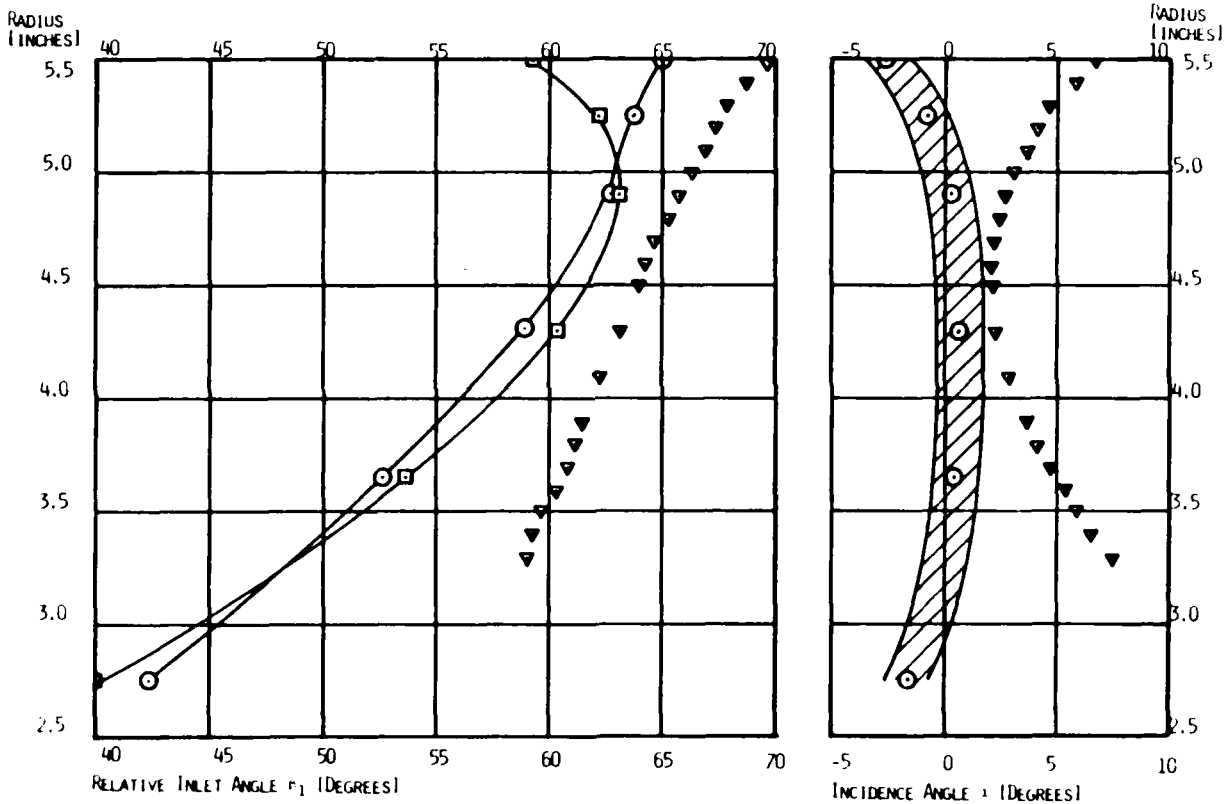

Figure 6. Required radial distribution of rotor relative inlet angle (β_1) and incidence angle (i) compared with measurements.

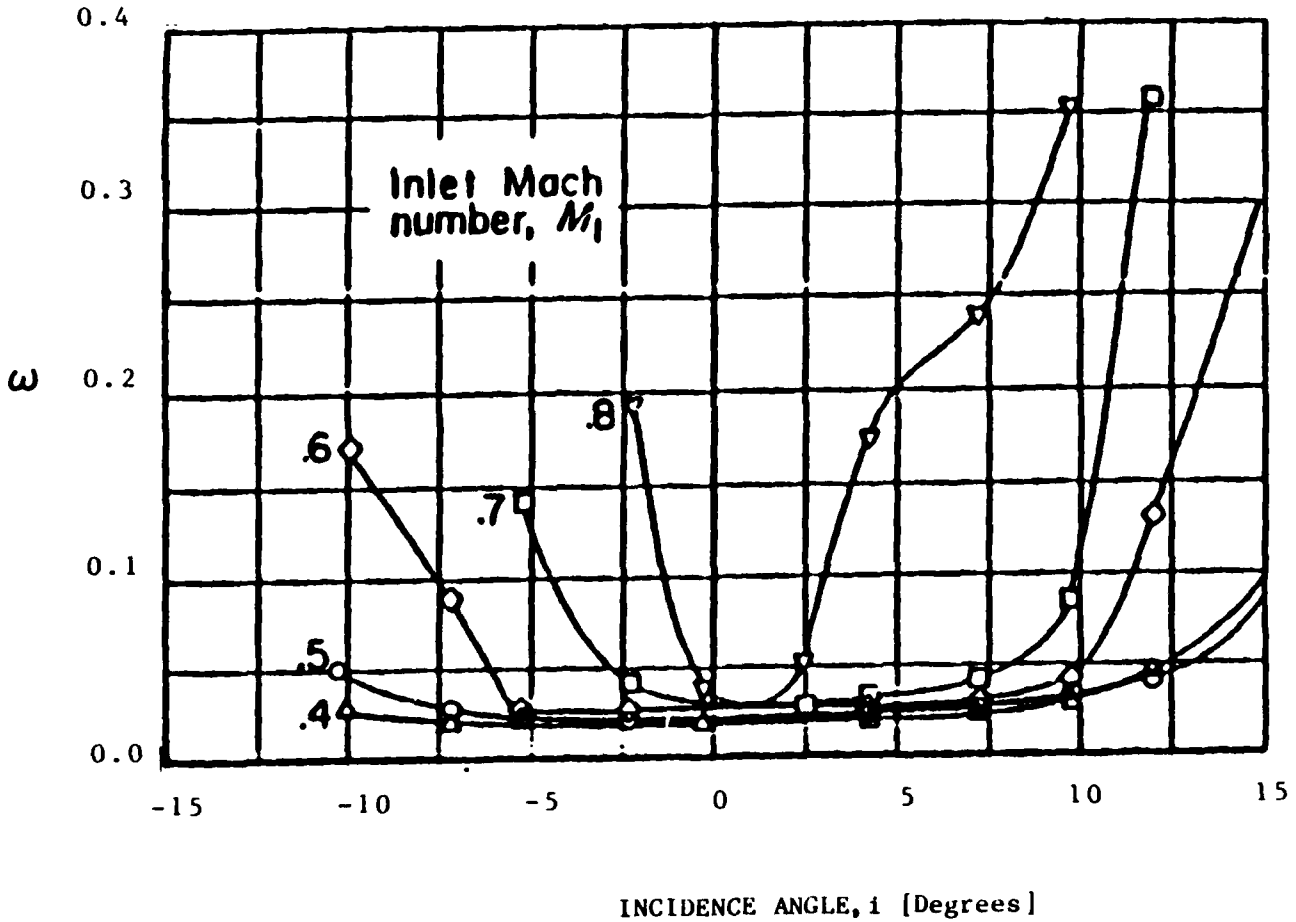

Figure 7. Total pressure-loss coefficient ω_t versus incidence angle depending on inlet Mach number for a circular-arc blade. Camber angle, 25°; maximum thickness ratio, 0.10; solidity, 1.333; blade chord angle, 42.5°. (Reproduced from Fig. 130a), NASASP-36, N65-23345.

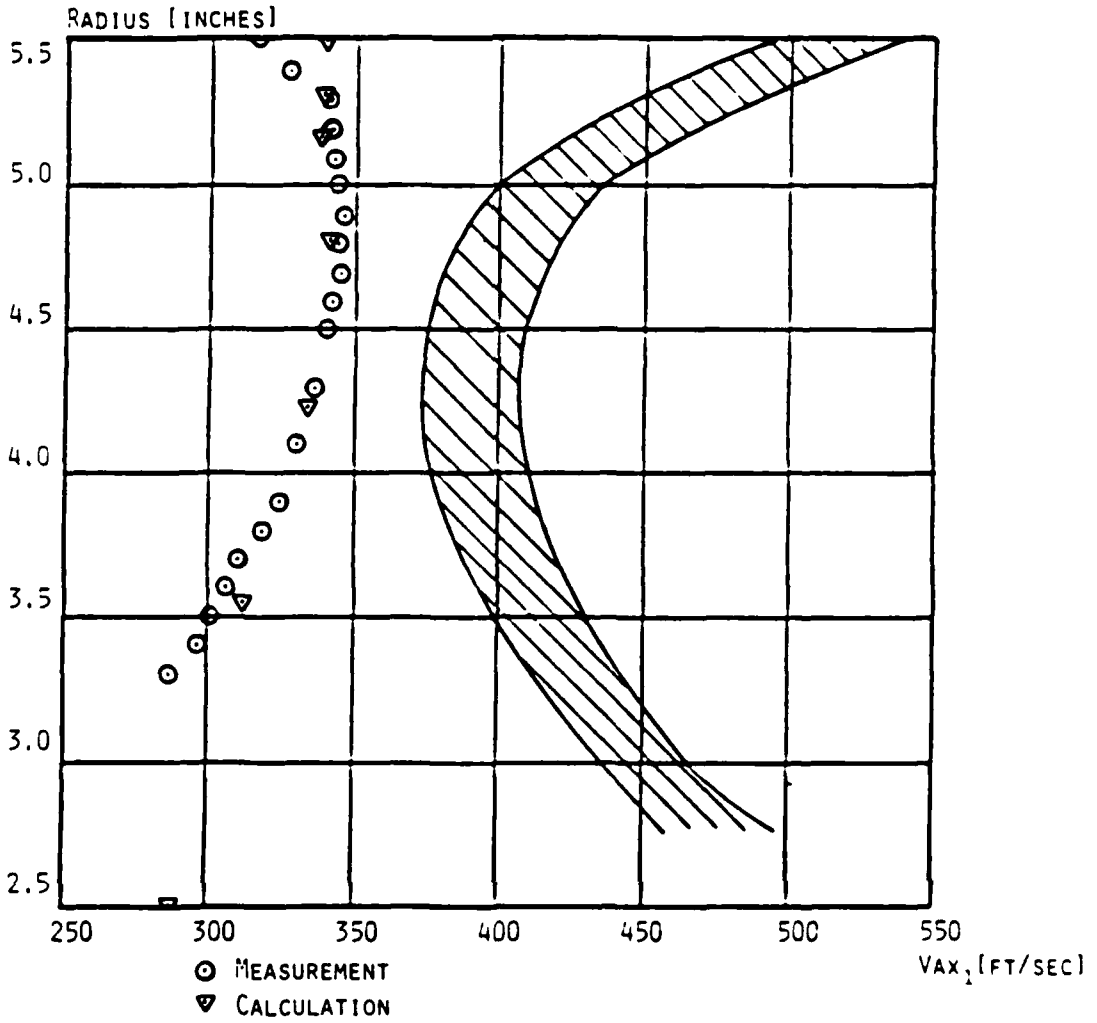

Figure 8. Comparison of measured and calculated radial distribution of V_{AX_1} with range of V_{AX_1} required for optimum incidence (shaded).

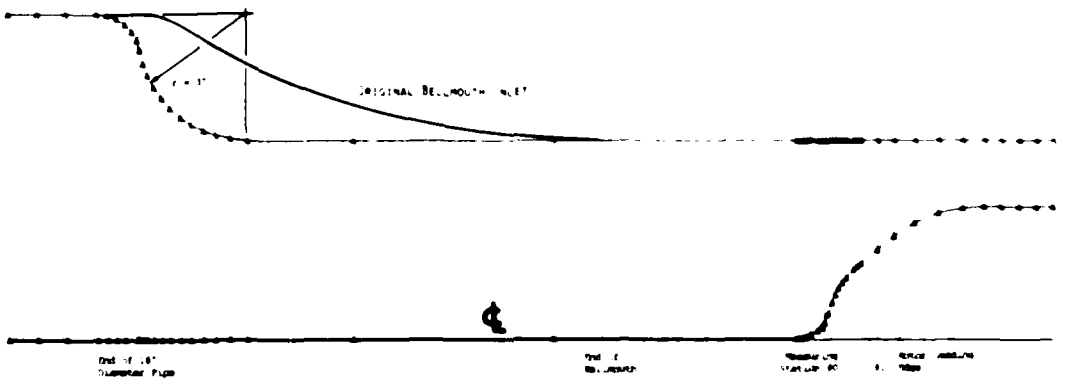

Figure 9. Computation region for small radius inlet contraction.

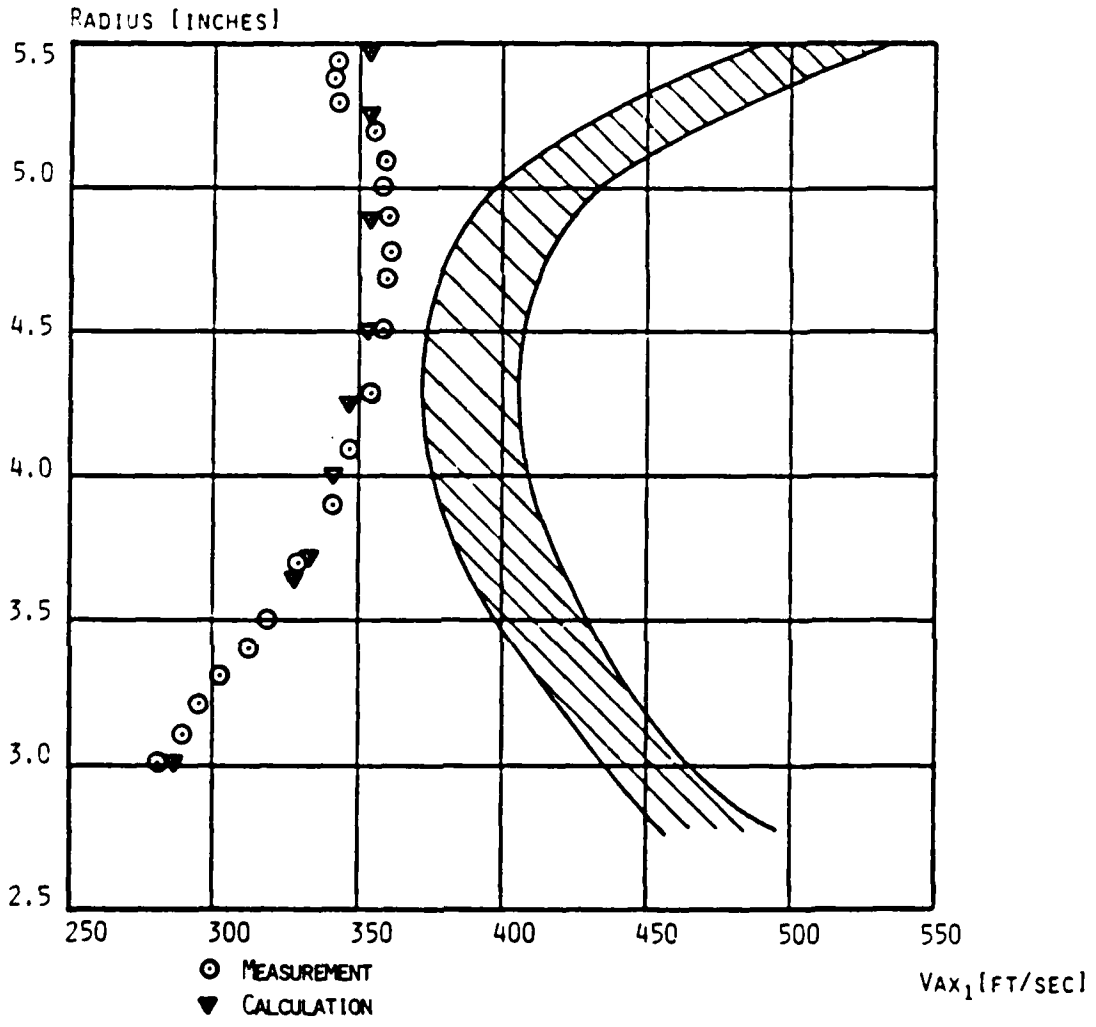

Figure 10. Comparison of measured and calculated radial distributions of V_{AX_1} for small radius inlet contraction with range of V_{AX_1} required for optimum incidence (shaded).

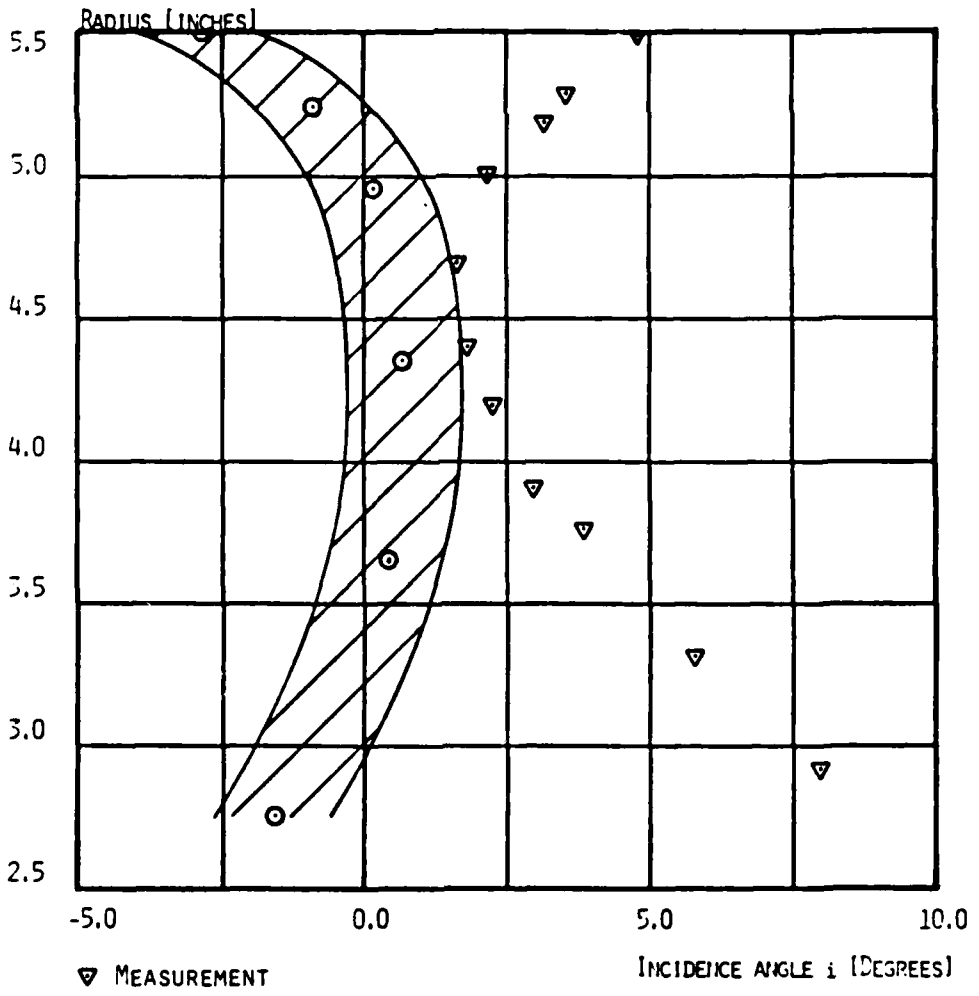

Figure 11. Measured radial distribution of incidence angle compared to optimum range of incidence (shaded).

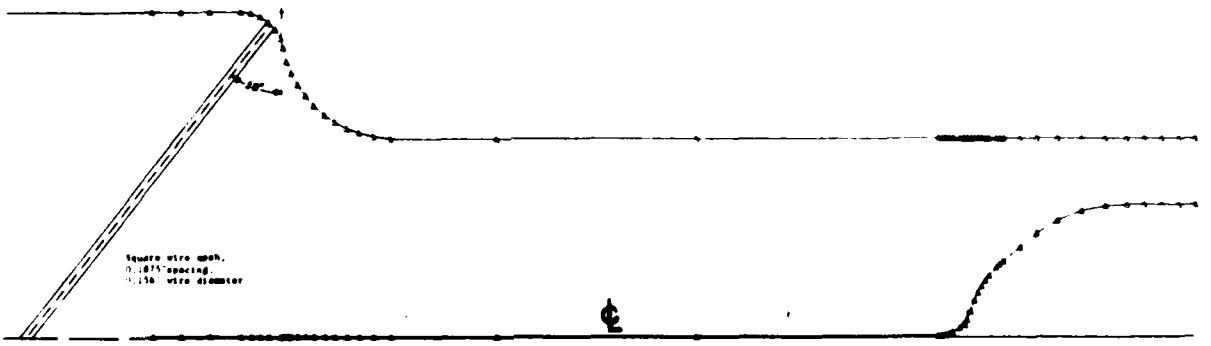

Figure 12. Small radius inlet contraction with conical screen. (Not to scale).

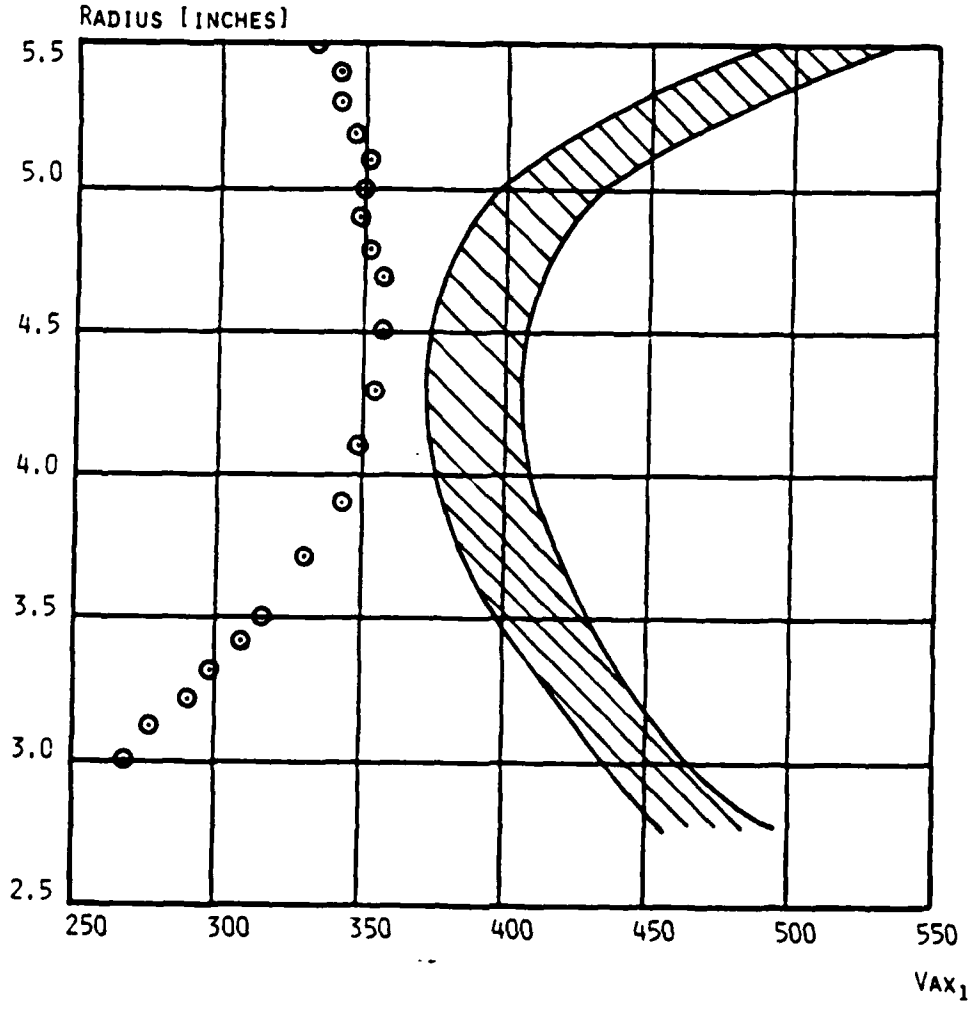

Figure 13. Comparison of measured radial distribution of V_{AX_1} with range of V_{AX_1} required for optimum incidence (shaded) for the small radius inlet contraction, including a conical screen.

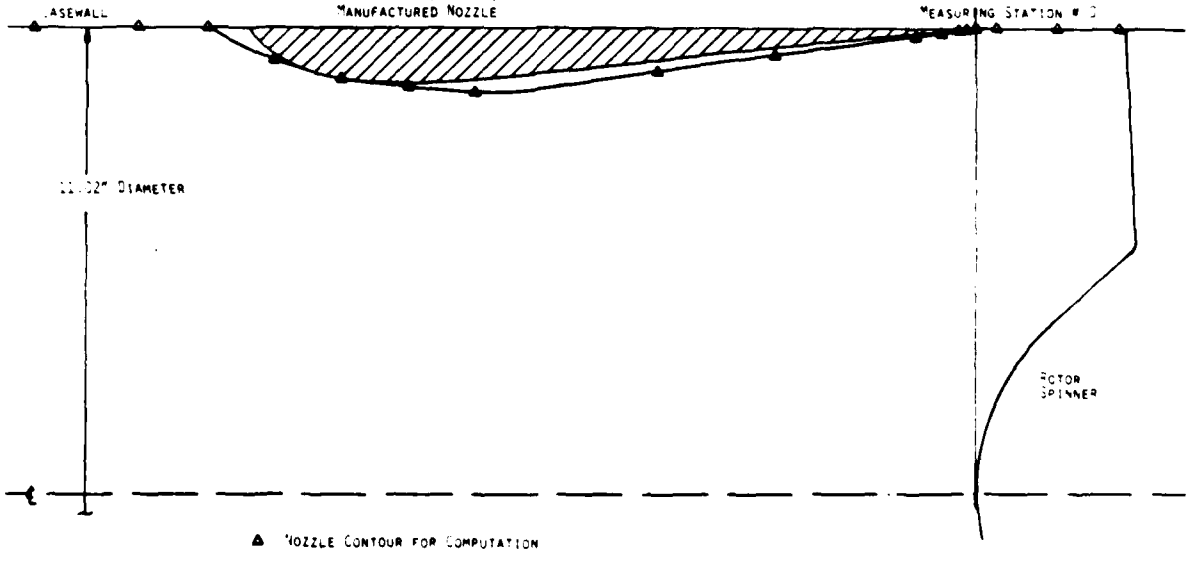

Figure 14. Contracting nozzles in the compressor inlet ahead of the rotor leading edge.

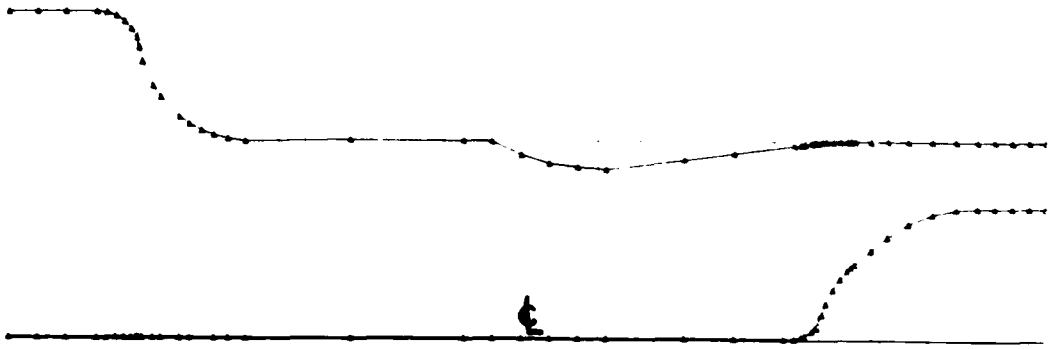

Figure 15. Computation region for the contracting nozzle configuration.

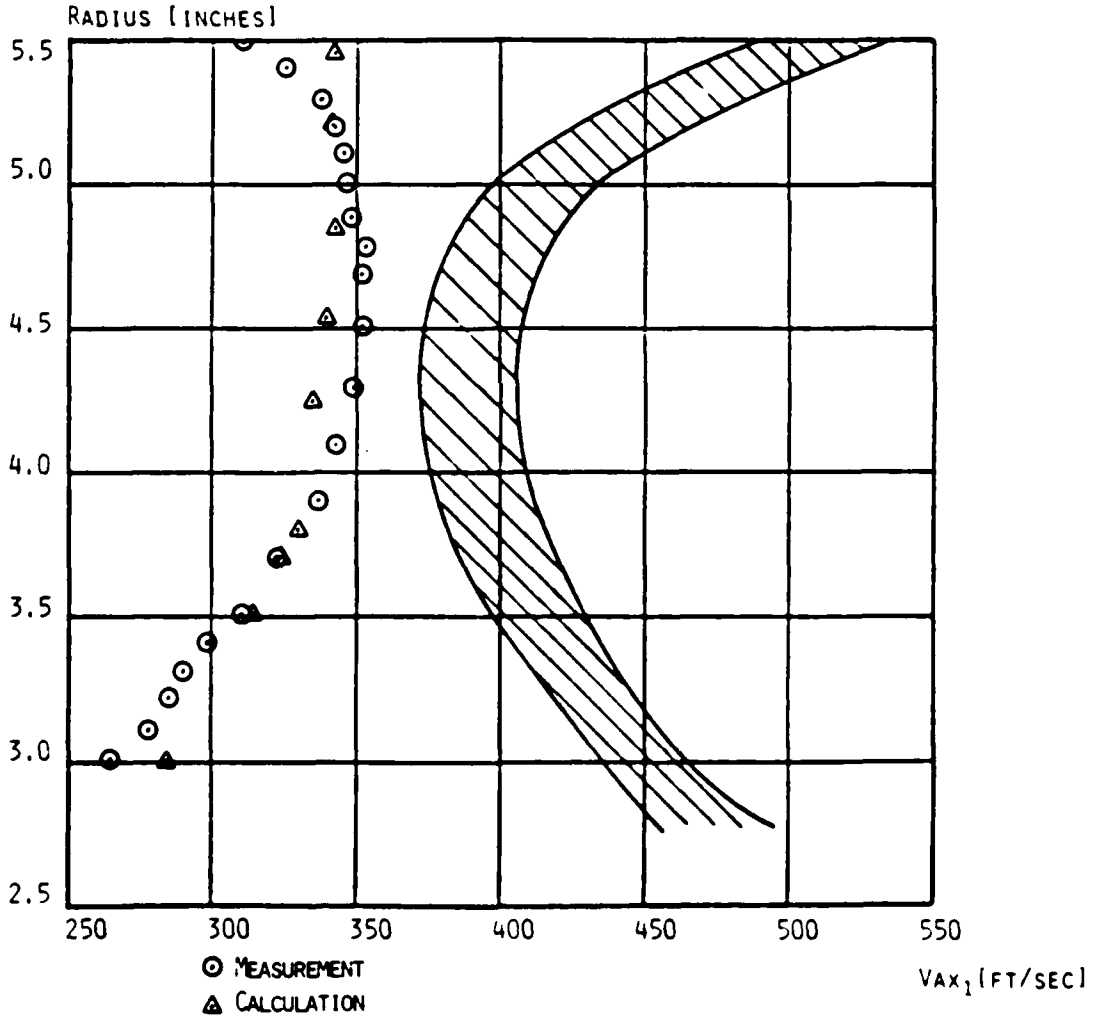

Figure 16. Comparison of measured and calculated radial distributions of V_{AX1} with range of V_{AX1} required for optimum incidence (shaded) for a contracting nozzle in the inlet.

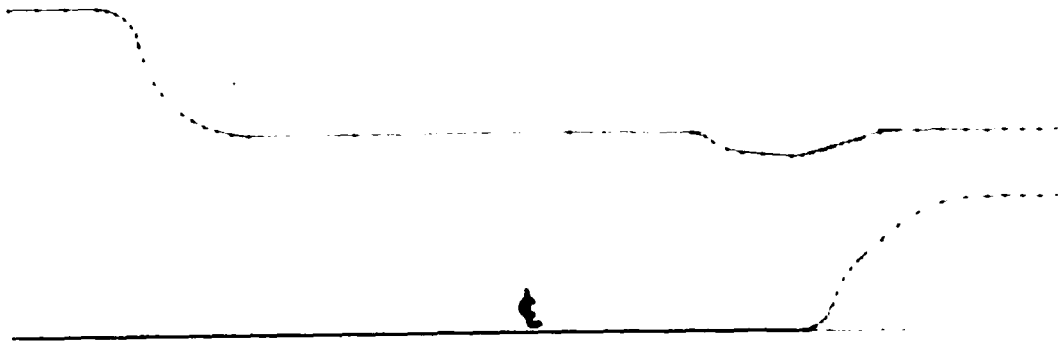

Figure 17. Computation region for constant cross-sectional area nozzle ahead of the leading edge.

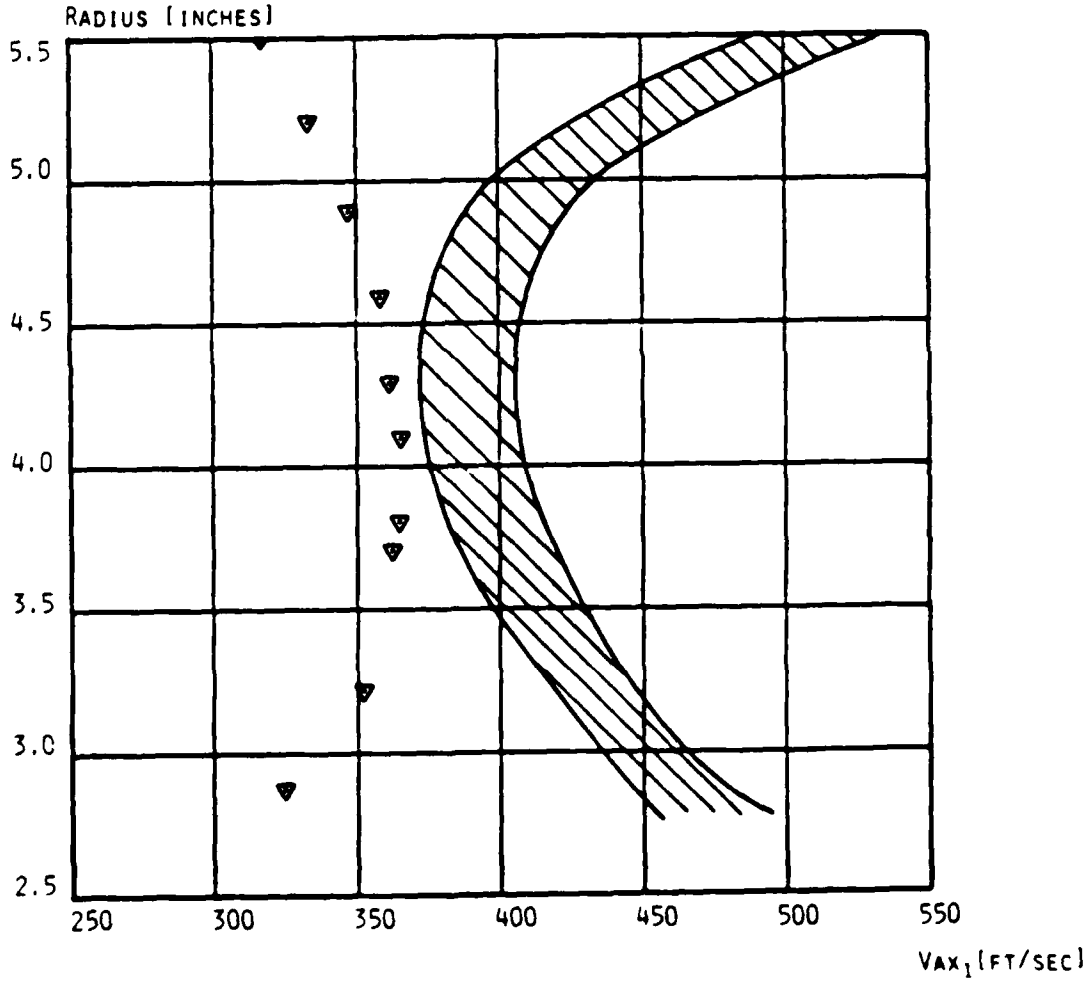

Figure 18. Comparison of the calculated radial distribution of V_{AX_1} with the range of V_{AX_1} required for optimum incidence (shaded), for the nozzle shown in Figure 17.

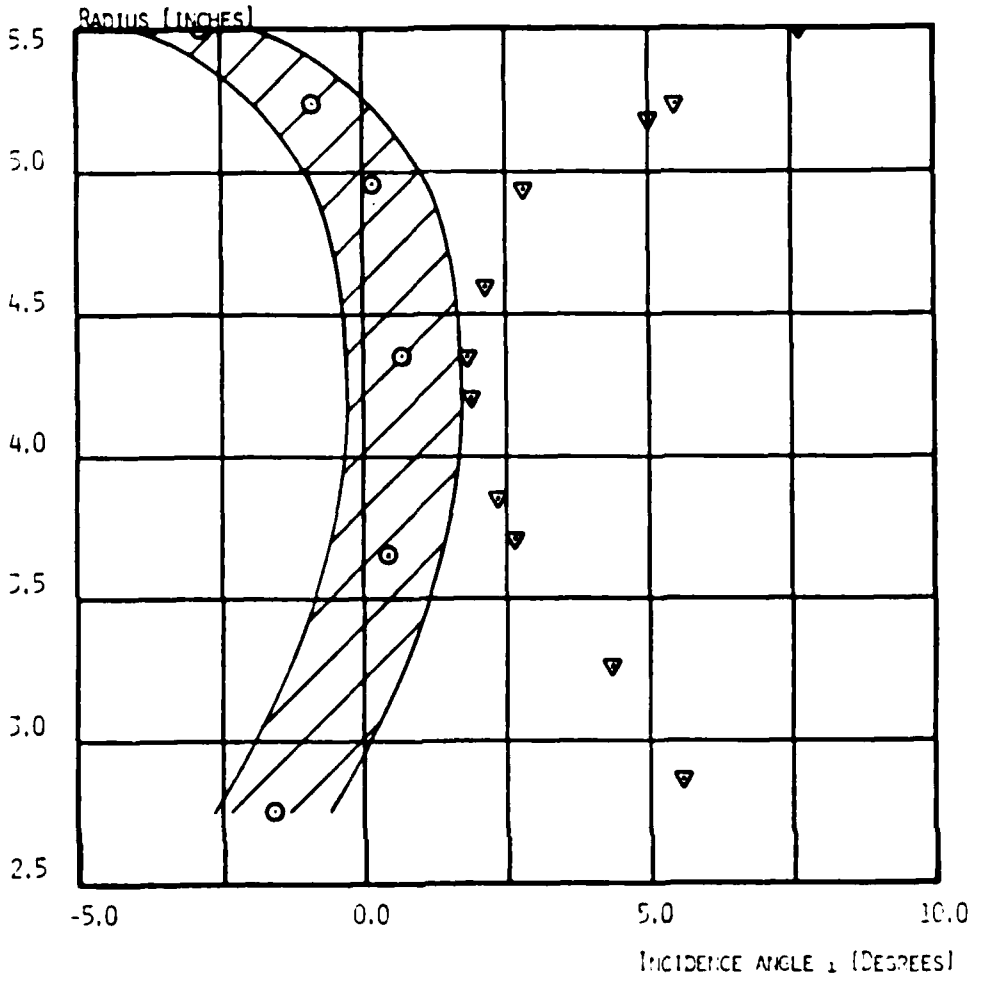

Figure 19. Comparison of the calculated radial distribution of incidence angle (▽) with the optimum (⊙) range of incidence (shaded).

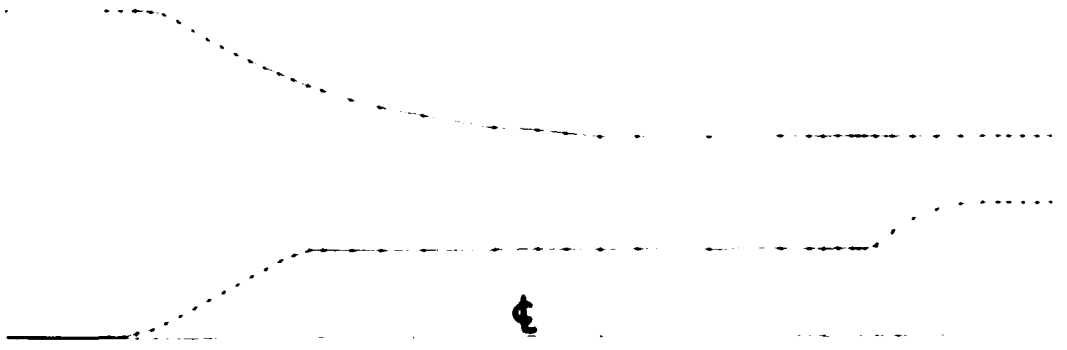

Figure 20. Computation region for the compressor inlet with a centerbody.

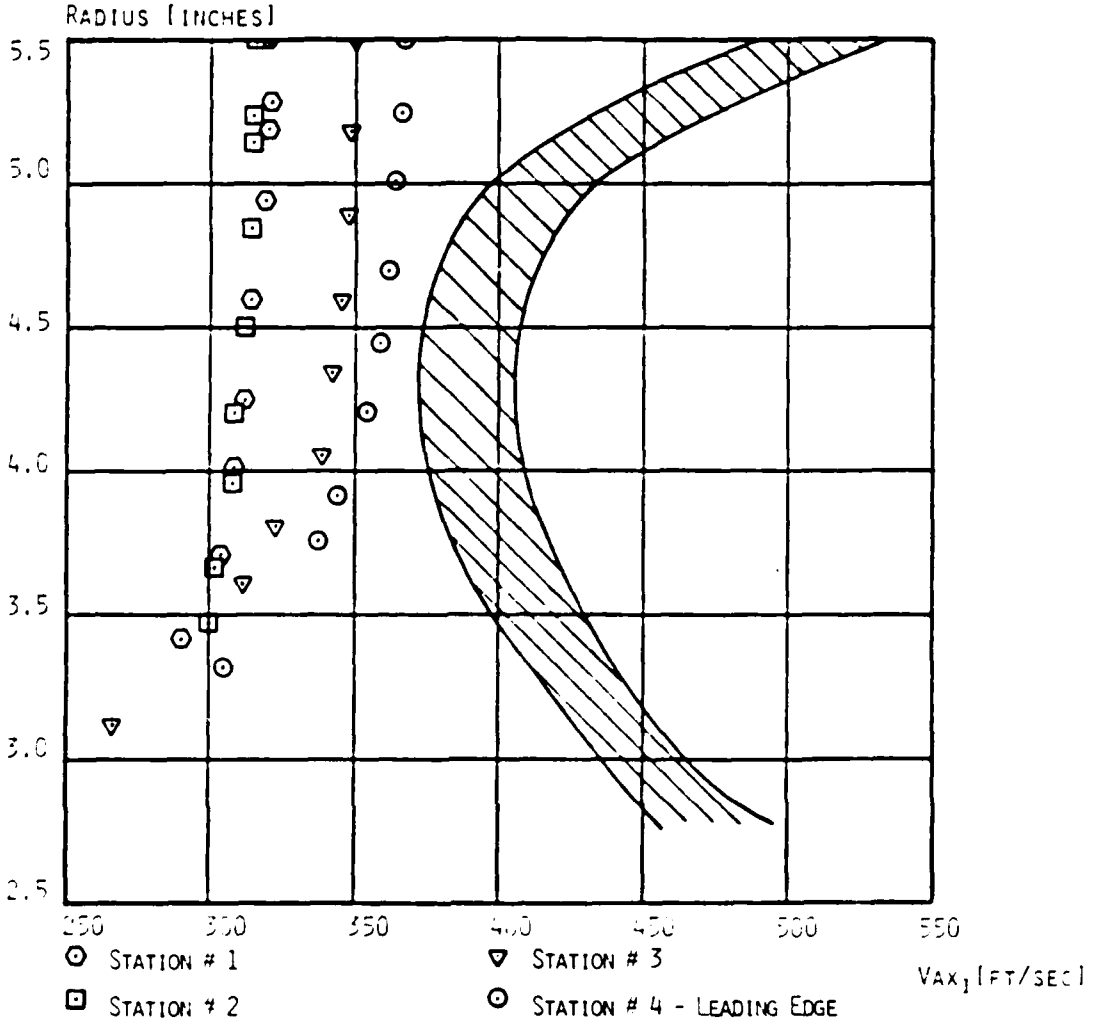

Figure 21. V_{AX_1} calculated at stations upstream of the rotor for the centerbody in Figure 20 compared with the range of V_{AX_1} required for optimum incidence at the rotor face (shaded).

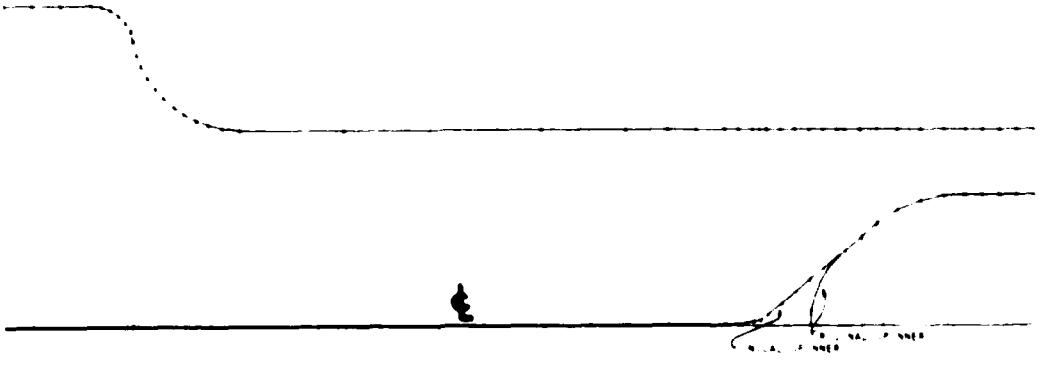

Figure 22. Computation region for a conical spinner.

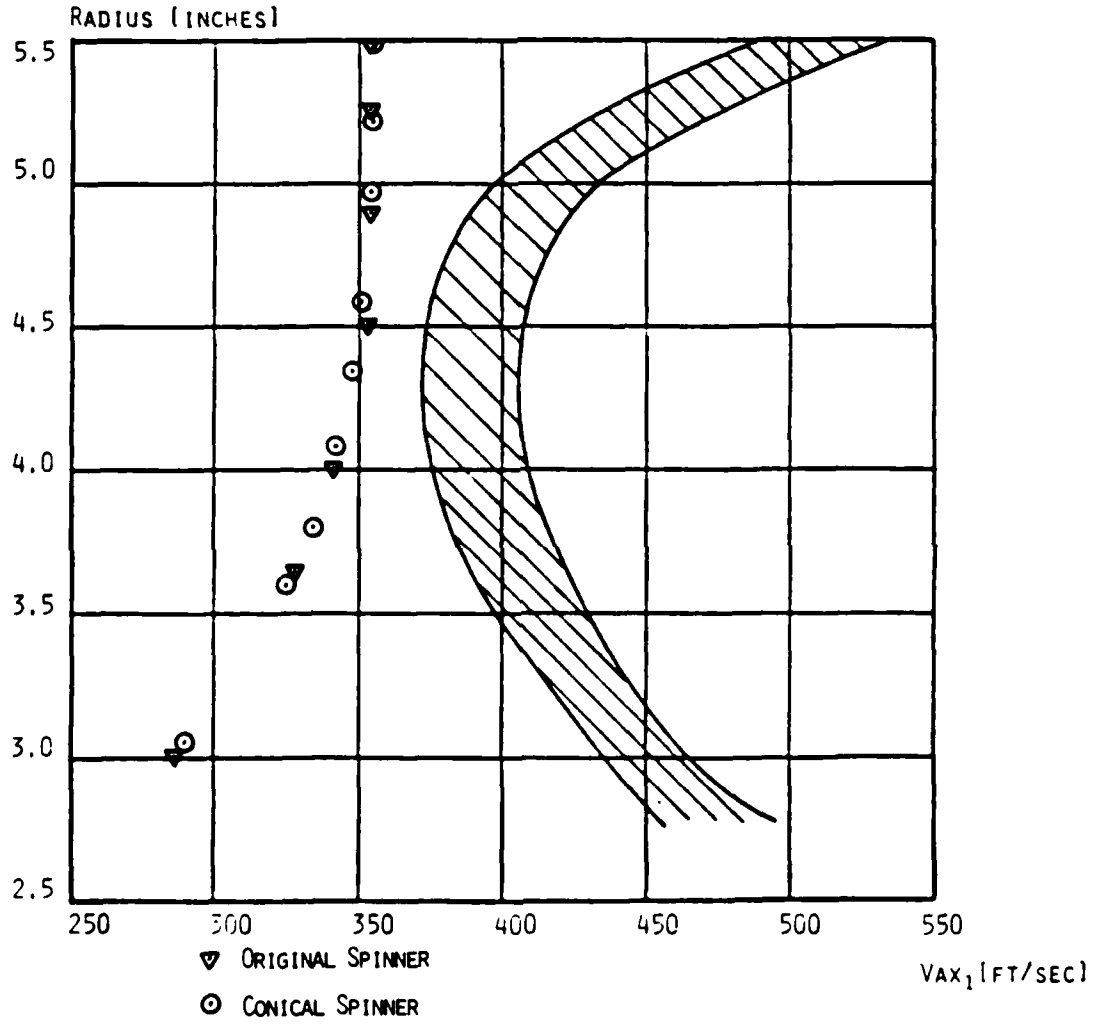

Figure 23. Comparison of calculated radial distributions of V_{AX_1} for original and conical spinners and range of V_{AX_1} required for optimum incidence (shaded).

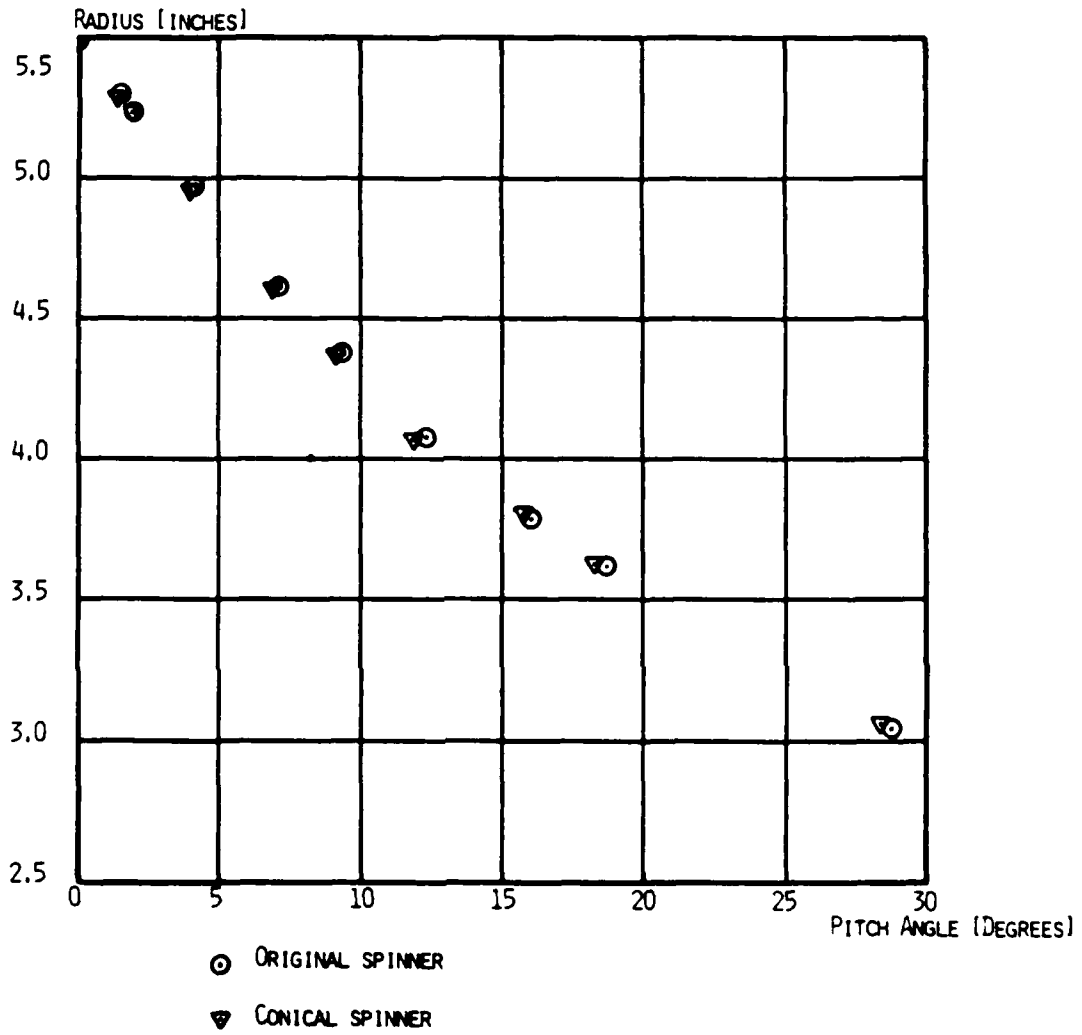

Figure 24. Comparison of radial distribution of pitch angles calculated for the original and the conical spinner.

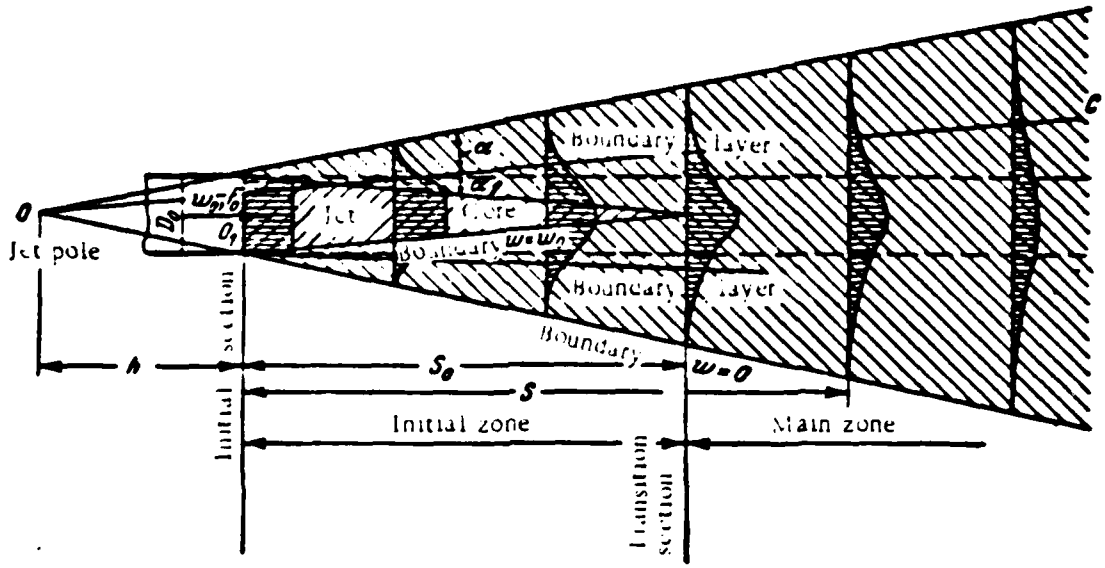

Figure 25. Structure of a free jet. (Reproduced Figure 11-4, page 409, Handbook of Hydraulic Resistance, I.E. Idel'chik.)

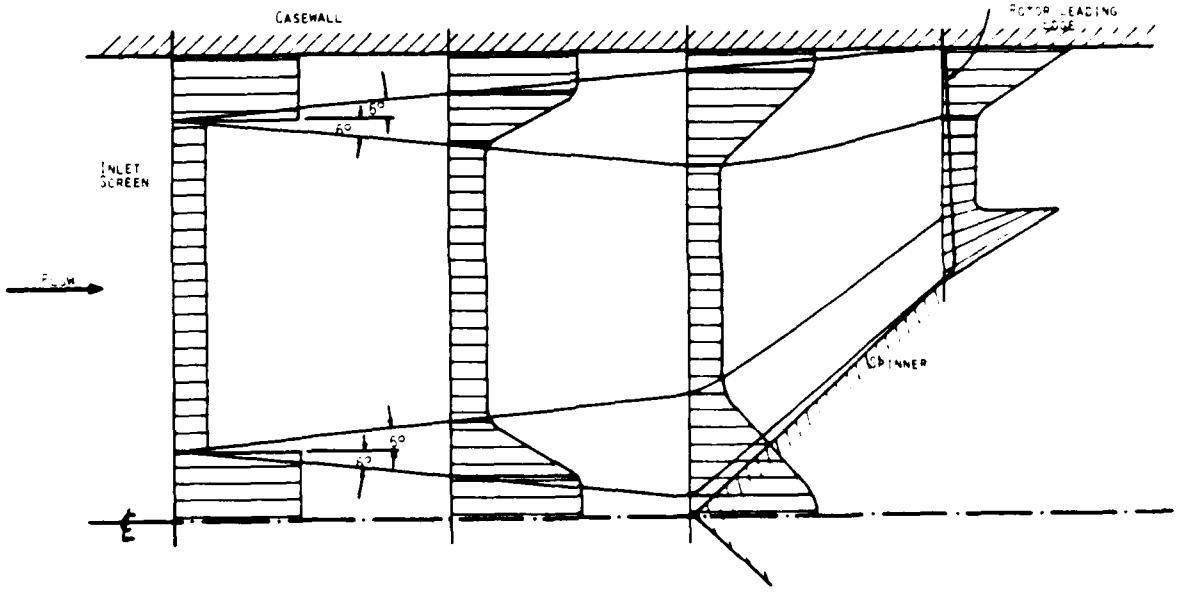

Figure 26. High speed-low speed plume mixing schematic.

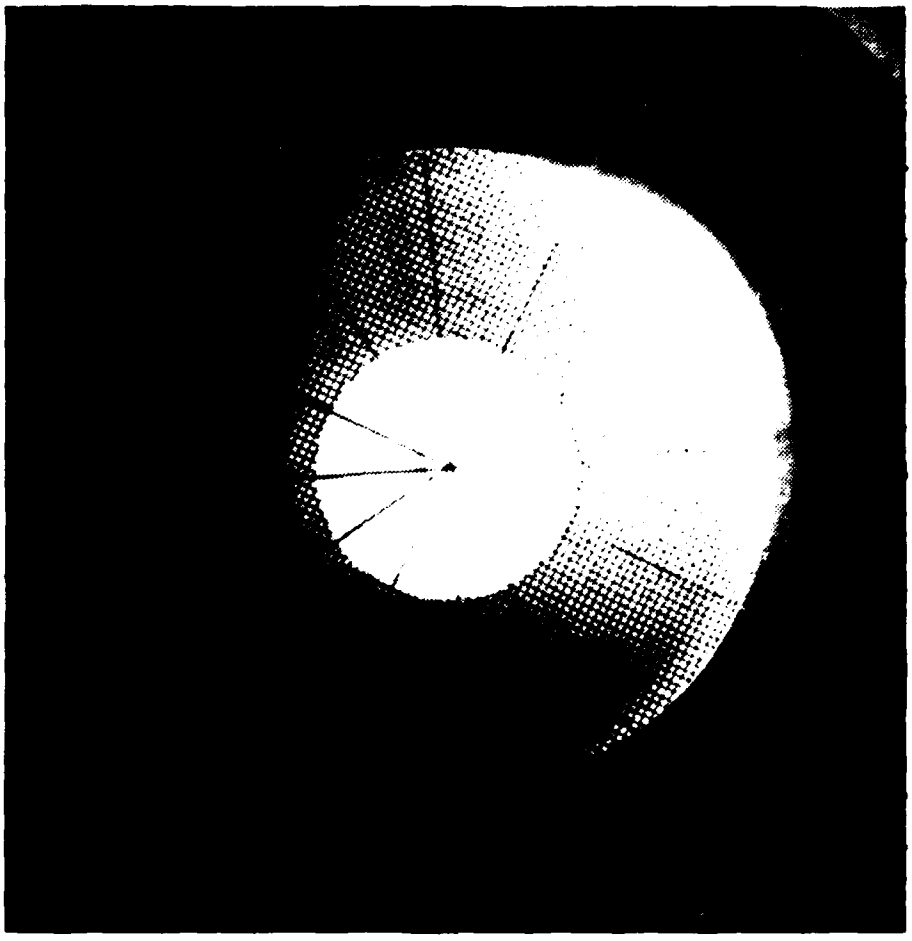

Figure 27. First inlet screen installed in inlet ducting.

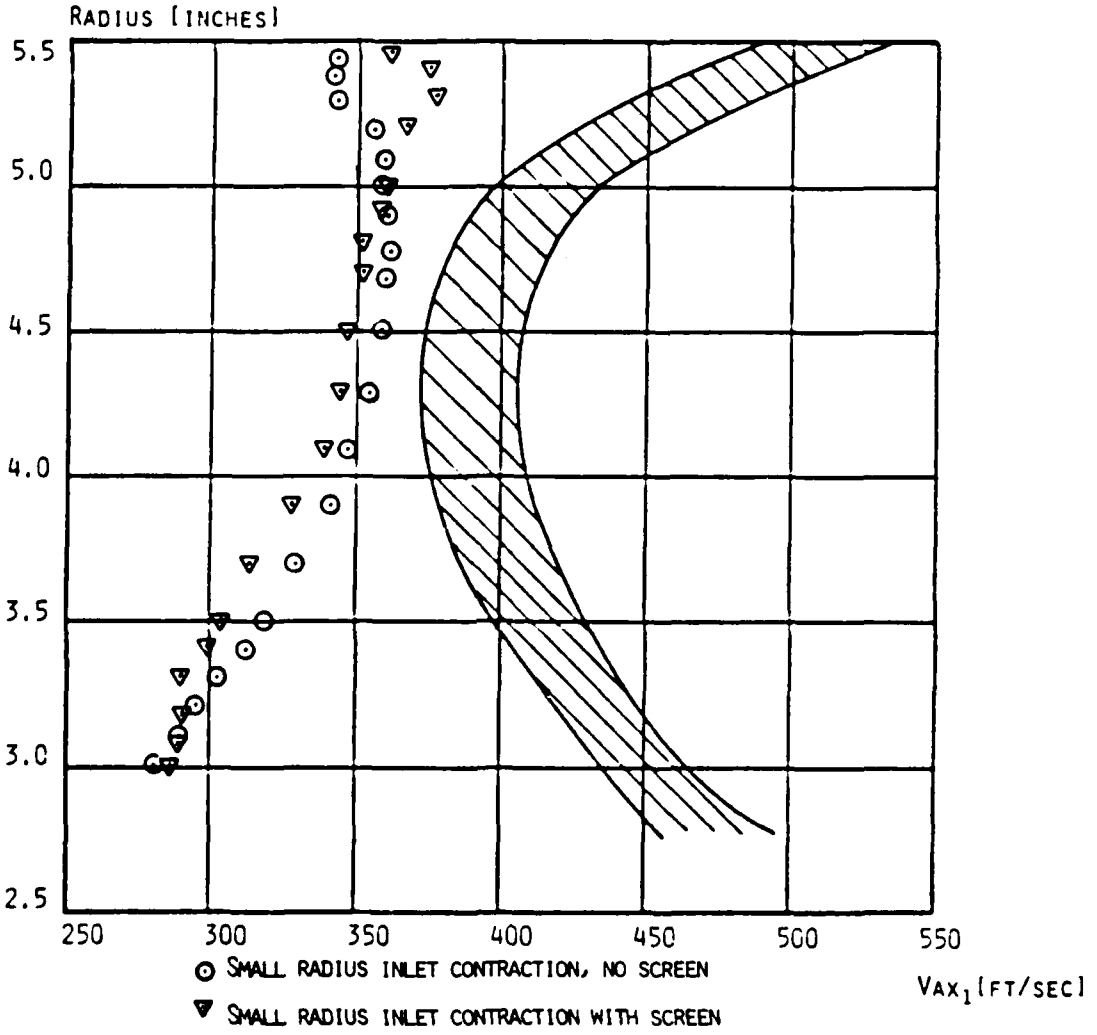

Figure 28. Measured distribution of V_{AX1} versus radius for an identical inlet with and without a screen.

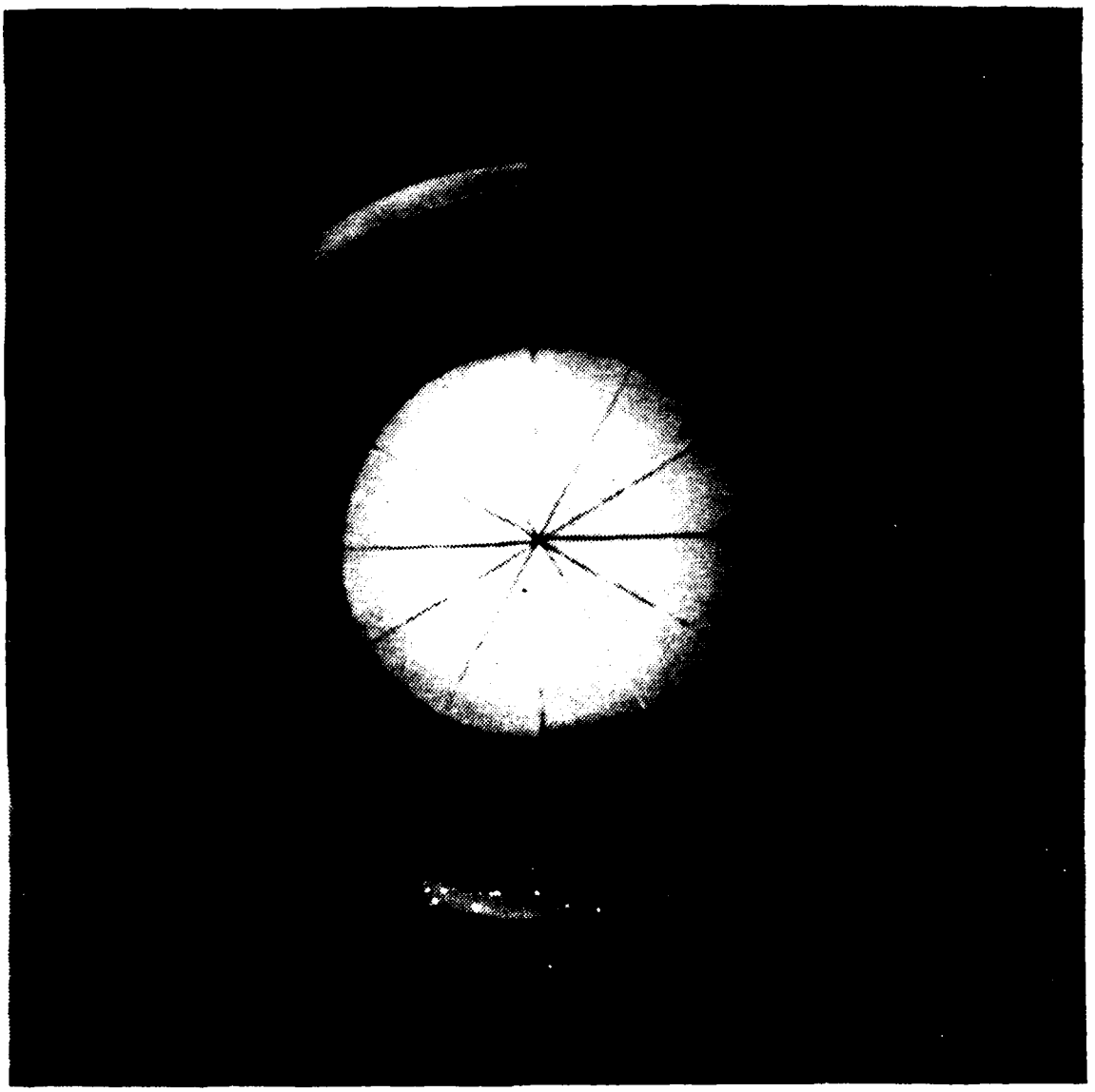

Figure 29. Second inlet screen installed in inlet ducting.

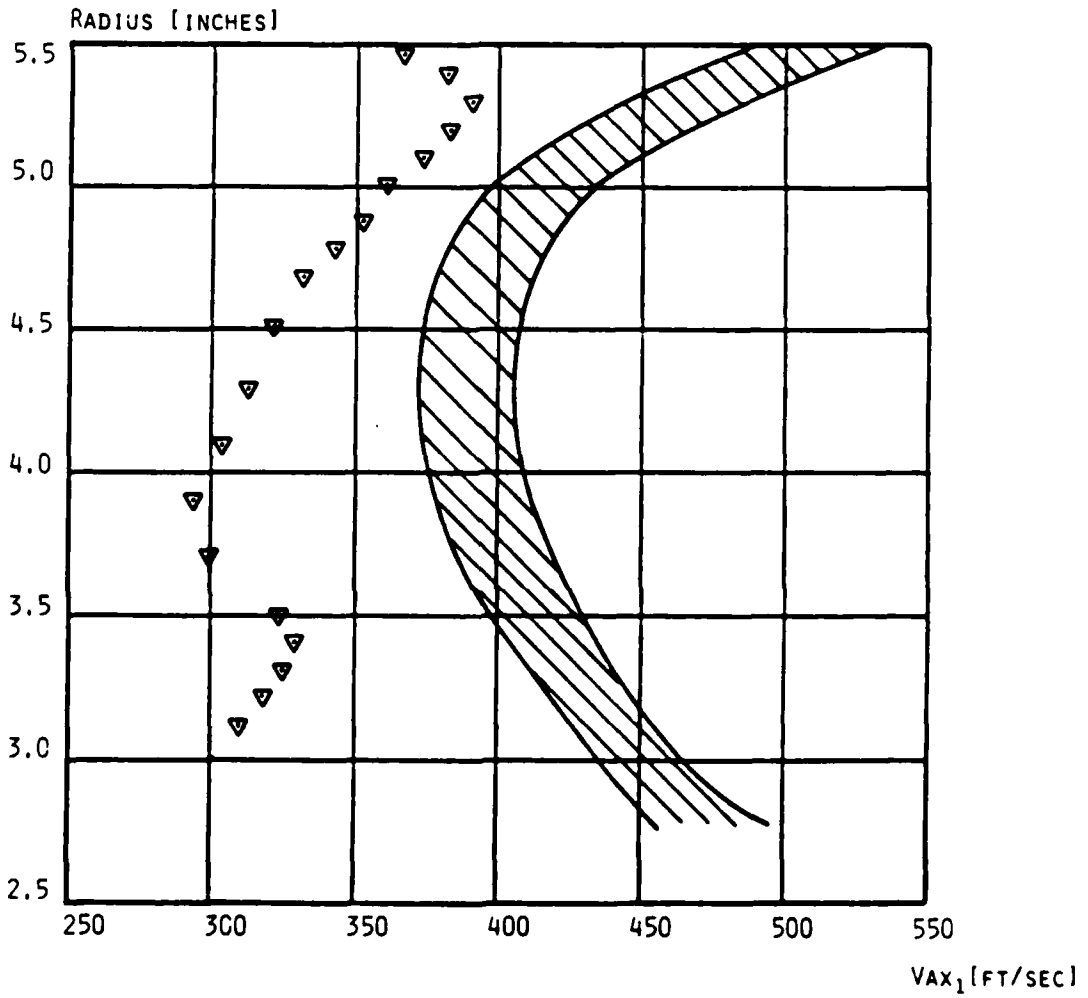

Figure 30. Measured radial distribution of V_{AX1} with the second inlet screen shown in Figure 29. (Range for optimum incidence is shaded)

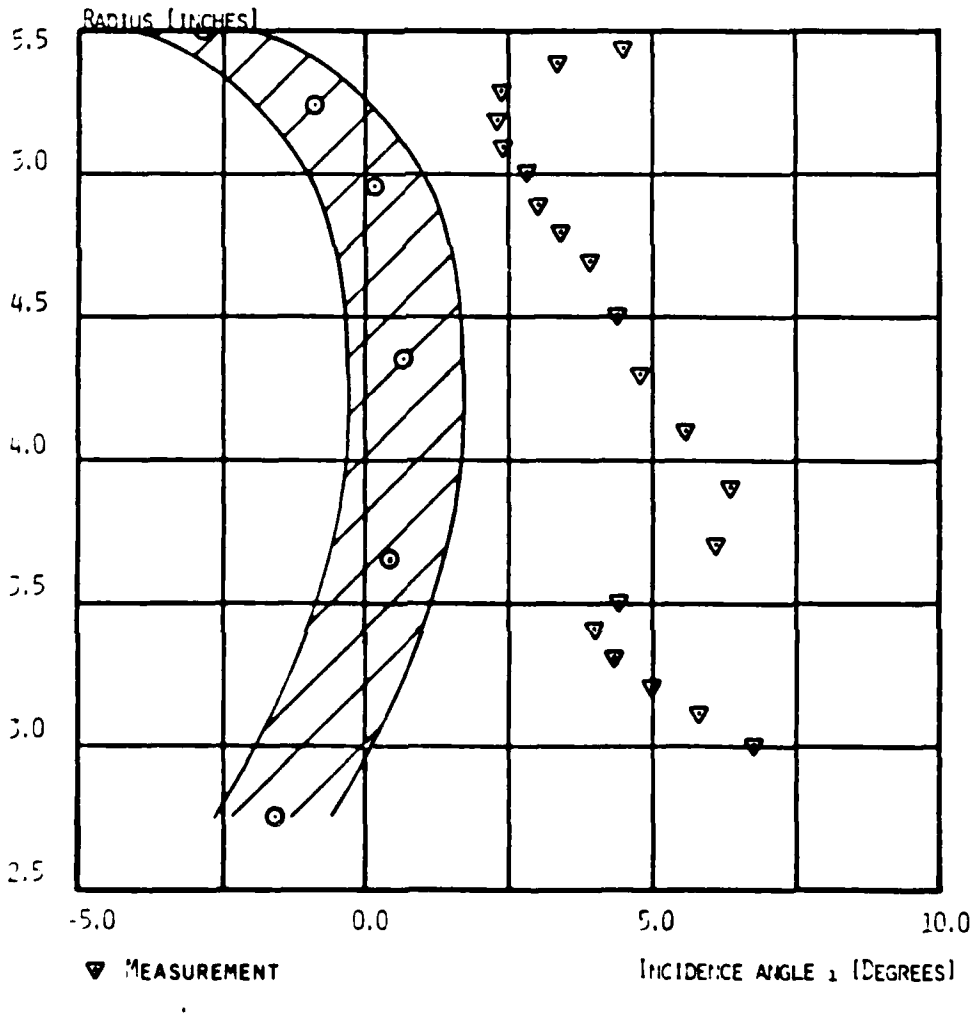

Figure 31. Measured radial distribution of incidence with the second inlet screen. (Optimum range of incidence is shaded.)

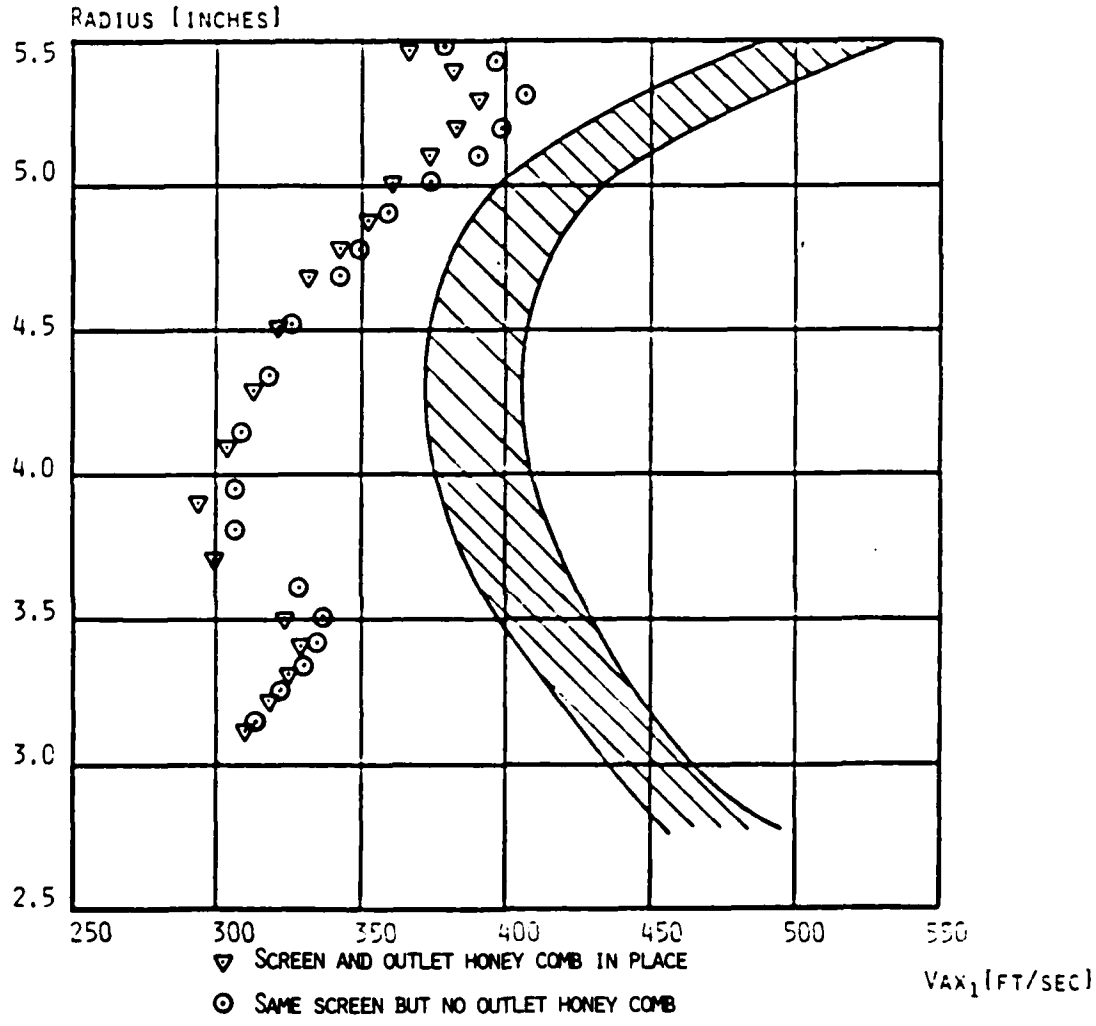

Figure 32. Comparison of measured radial distribution of V_{AX1} with and without exit honeycomb installed, with second inlet screen. (Range for optimum incidence is shaded.)

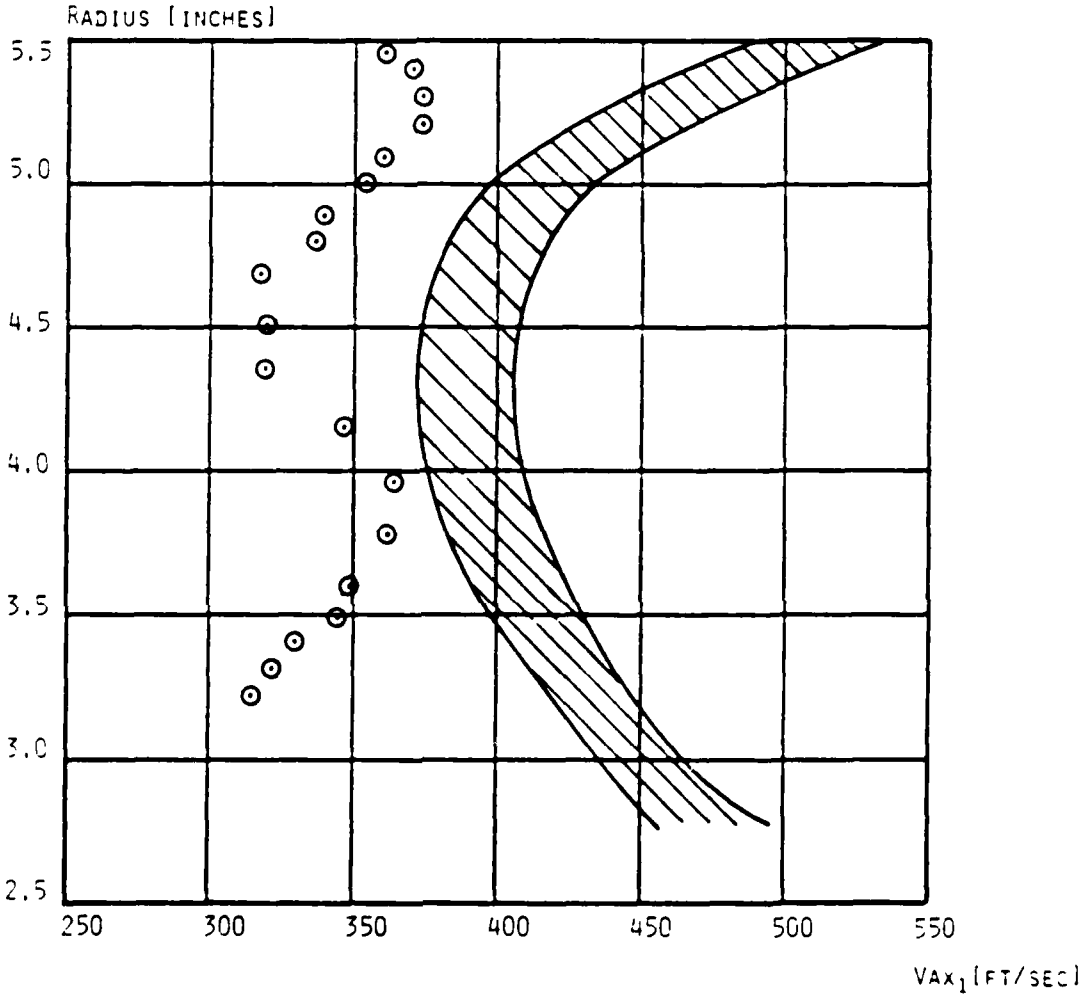

Figure 33. Measured radial distribution of V_{AX1} with the third inlet screen installed. (Range for optimum incidence is shaded.)

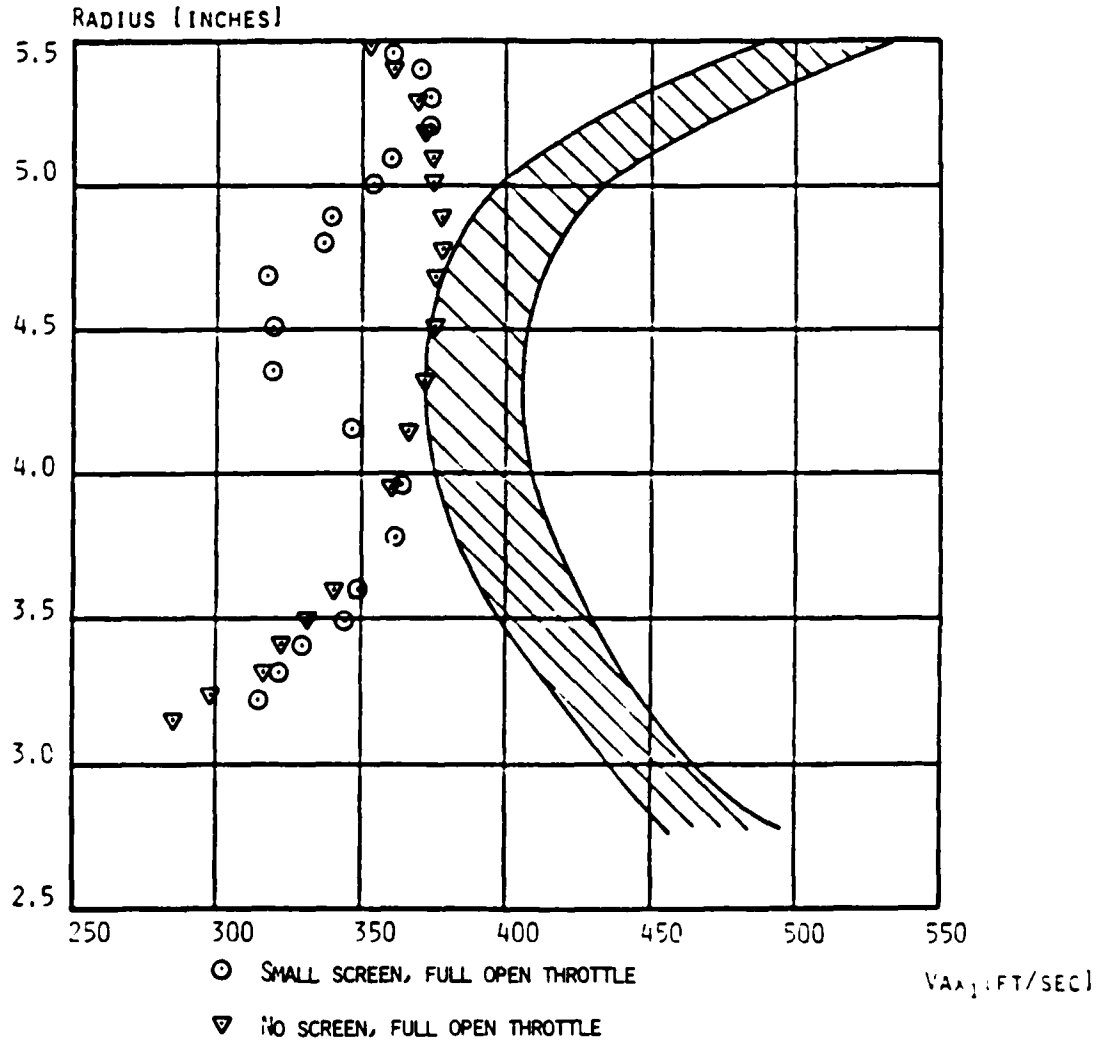

Figure 34. Comparison of measured radial distribution of V_{AX1} with the third inlet screen and without a screen installed. (Range for optimum incidence is shaded.)

References

1. Erwin, J. R., "A Review of the Design of the NPS/TPL Transonic Compressor", Naval Postgraduate School Contractor Report, NPS67-83-004CR, March 1983.

2. Shreeve R. P. and Neuhoff, F., "Measurements of the Flow From a High Speed Compressor Rotor Using a Dual Probe Digital Sampling (DPDS) Technique", ASME, Journal of Engineering for Gas Turbines and Power, Vol. 106, April 1984, PPS 366-375

3. Neuhoff, F., "Calibration and Application of a Combination Temperature-Pneumatic Probe for Velocity and Rotor Loss Distribution Measurements in a Compressor", Naval Postgraduate School Contractor Report NPS67-81-03CR, December 1981.

4. Aerodynamic Design of Axial-Flow Compressors NASA SP-36, N65-23345.

5. Katsanis, T. and M^{c}Nally, W. D., "Revised Fortran Program for Calculating Velocities and Streamlines on the Hub-Shroud Mid Channel Stream Surface of an Axial-, Radial-, or Mixed -Flow Turbomachine or Annular Duct. NASA TND-8430.

6. Idel'chik, I. E., Handbook of Hydraulic Resistance, Israel Program for Scientific Translations Ltd., 1966

DISTRIBUTION LIST

1. Commander
   Naval Air Systems Command
   Washington, DC 20361
   Attention: Code AIR 931 E — 1
   Code AIR 530 — 1
   Code AIR 536 — 1
   Code AIR 00D — 14

2. Commanding Officer
   Naval Air Propulsion Center
   Trenton, NJ 08628
   Attention: G. Mangano, PE-31 — 1

3. Commanding Officer — 1
   Naval Air Development Center
   Warminster, PA 19112
   Attention: AVTD

4. Library — 1
   Army Aviation Material Laboratories
   Department of the Army
   Fort Eustis, VA 23604

5. Dr. Arthur J. Wennerstrom — 1
   AFWAL/POTX
   Wright-Patterson AFB
   Dayton, OH 45433

6. National Aeronautics & Space Administration
   Lewis Research Center
   21000 Brookpark Road
   Cleveland, OH 44135
   Attention: Library — 1

7. Library — 1
   General Electric Company
   Aircraft Engine Technology Division
   DTO Mail Drop H43
   Cincinnati, OH 45215

8. Library — 1
   Pratt & Whitney Aircraft Group
   Post Office Box 2691
   West Palm Beach, FL 33402

9. Library — 1
   Pratt-Whitney Aircraft Group
   East Hartford, CT 06108

10. Library — 1
Curtis Wright Corporation
Woodridge, NJ 07075

11. Library — 1
AVCO/Lycoming
550 S. Main Street
Stratford, CT 06497

12. Library — 1
Teledyne CAE, Turbine Engines
1330 Laskey Road
Toledo, OH 43612

13. Library — 1
Williams International
P. O. Box 200
Walled Lake, MI 48088

14. Library — 1
Detroit Diesel Allison Division G.M.C.
P. O. Box 894
Indianapolis, IN 46202

15. Library — 1
Garrett Turbine Engine Company
111 S. 34th Street
P. O. Box 5217
Phoenix, AZ 85010

16. Professor Leonhard Fottner — 2
Department of Aeronautics and Astronautics
German Armed Forces University
Hochschule des Bundeswehr
Werner Heisenbergweg 39
8014 Neubiberg near Munich
WEST GERMANY

17. Defense Technical Information Center — 2
Cameron Station
Alexandria, VA 22314

18. Naval Postgraduate School
Monterey, CA 93943
Attn: Professor M. F. Platzer (67PL) — 1
Turbopropulsion Laboratory (67Sf) — 10
Research Adminstration (012) — 1
Library (1424) — 2

END

4-87

DTIC